iScience

CellPress

Article

2-Methylthio Conversion of N6-Isopentenyladenosine in Mitochondrial tRNAs by CDK5RAP1 Promotes the Maintenance of Glioma-Initiating Cells

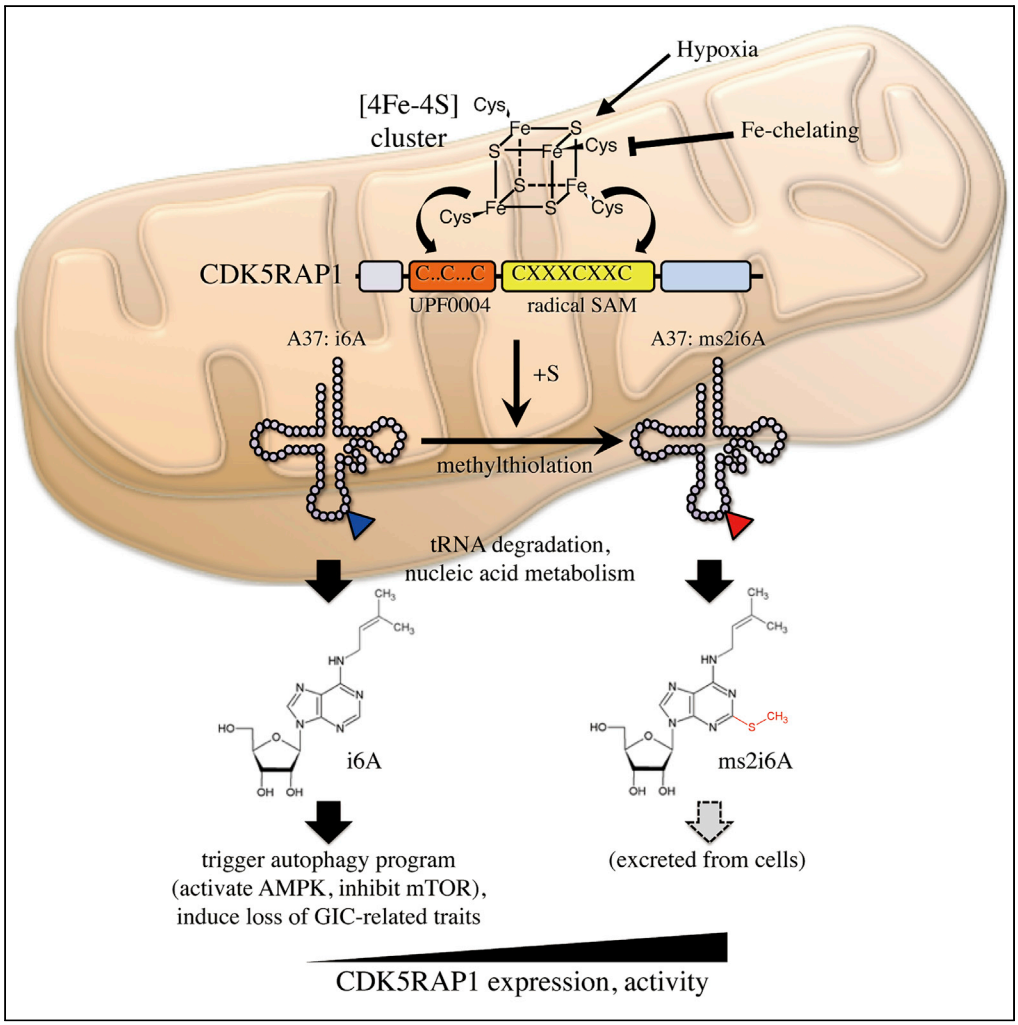

Takahiro Yamamoto, Atsushi Fujimura, Fan-Yan Wei, Naoki Shinojima, Jun-ichiro Kuroda, Akitake Mukasa, Kazuhito Tomizawa

tomikt@kumamoto-u.ac.jp

HIGHLIGHTS

CDK5RAP1 is required to sustain the growth of GICs through ms^2 modification of i^6A

Deficit of CDK5RAP1 inhibits the growth of GIC through i^6A accumulation

CDK5RAP1 detoxifies i^6A by conversion into ms^2i^6A in the mitochondria of GICs

Mitochondria serve as antidotal machinery against i^6A in GICs

Yamamoto et al., iScience *21*, 42–56
November 22, 2019 © 2019 The Author(s).
https://doi.org/10.1016/j.isci.2019.10.012

iScience

CellPress

Article

2-Methylthio Conversion of N6-Isopentenyladenosine in Mitochondrial tRNAs by CDK5RAP1 Promotes the Maintenance of Glioma-Initiating Cells

Takahiro Yamamoto,[1,2,6] Atsushi Fujimura,[1,4,5,6] Fan-Yan Wei,[1] Naoki Shinojima,[2] Jun-ichiro Kuroda,[2] Akitake Mukasa,[2] and Kazuhito Tomizawa[1,3,5,*]

SUMMARY

2-Methylthio-N^6-isopentenyl modification of adenosine (ms^2i^6A) is an evolutionally conserved modification found in mitochondrial (mt)-tRNAs. Cdk5 regulatory subunit-associated protein 1 (CDK5RAP1) specifically converts N6-isopentenyladenosine (i^6A) to ms^2i^6A at position A37 of four mt-DNA-encoded tRNAs, and the modification regulates efficient mitochondrial translation and energy metabolism in mammals. Here, we report that the ms^2 conversion mediated by CDK5RAP1 in mt-tRNAs is required to sustain glioma-initiating cell (GIC)-related traits. CDK5RAP1 maintained the self-renewal capacity, undifferentiated state, and tumorigenic potential of GICs. This regulation was not related to the translational control of mt-proteins. CDK5RAP1 abrogated the antitumor effect of i^6A by converting i^6A to ms^2i^6A and protected GICs from excessive autophagy triggered by i^6A. The elevated activity of CDK5RAP1 contributed to the amelioration of the tumor-suppressive effect of i^6A and promoted GIC maintenance. This work demonstrates that CDK5RAP1 is crucial for the detoxification of endogenous i^6A and that GICs readily utilize this mechanism for survival.

INTRODUCTION

In cancer biology, mitochondria are key organelles for understanding the behavior of cancer cells. Mitochondria are involved in fine-tuning cellular metabolism, oxygen consumption, and energy production, and they control cell death programs such as apoptosis (Cogliati et al., 2016; Pernas and Scorrano, 2016). Moreover, mitochondria play key roles in cancer stem cells (CSCs), which are believed to confer histopathological heterogeneity and drug and/or radiation resistance in cancer tissues. The structure and dynamics of mitochondria are related to CSC-related traits such as self-renewal capacity and tumorigenic potential (Guha et al., 2014; Xie et al., 2015), and the translation of mitochondrial (mt) DNA-encoded genes can be a potential target for anticancer drugs (Skrtić et al., 2011). However, our knowledge regarding the molecular mechanism underlying the mitochondrial control of CSC fate is limited.

Nucleoside modifications have two roles in cancer biology: as an input for cellular decisions and as an output from nucleotide metabolism. The former is known to control cell growth and differentiation through epigenetic regulation (Brien et al., 2016; Lacadie et al., 2016; Zaidi et al., 2014), whereas the latter is known as a by-product of nucleotide metabolism. However, previous studies have shown that modified nucleosides can regulate the fate of cancer cells. When artificially applied, N6-isopentenyladenosine (i^6A), a modified nucleoside derived from tRNAs, induces cell-cycle arrest and cell death in many types of cancer cells, including glioblastoma cells (Castiglioni et al., 2013; Ciaglia et al., 2017; Laezza et al., 2009; Rajabi et al., 2010; Ranieri et al., 2018). Nevertheless, whether endogenous i^6A exerts the same effect and inhibits tumor growth remains unknown. Endogenous i^6A may also attenuate antitumor effects on cancer cells.

i^6A modifications exist only on the adenosine at position 37, which is a nucleotide neighboring the anticodon region in tRNAs (Wei et al., 2015). TRIT1 is an isopentenyl transferase that converts A into i^6A in mammals (Schweizer et al., 2017). Moreover, i^6A is converted to 2-methylthio (ms^2) i^6A (ms^2i^6A) by cyclin-dependent kinase 5 regulatory subunit associated-protein 1 (CDK5RAP1) in the mitochondria of mammalian cells (Wei et al., 2015). CDK5RAP1, a mitochondria-localizing methylthio-modifying enzyme, is essential for the conversion of i^6A to ms^2i^6A in mt-RNAs that read codons for Trp, Tyr, Phe, and Ser (Wei et al., 2015). This enzyme contributes to the maintenance of cellular respiration and metabolism in skeletal and cardiac muscles via the precise translation of mt-DNA-encoded genes. Therefore, CDK5RAP1 deficiency reduces

[1]Department of Molecular Physiology, Faculty of Life Sciences, Kumamoto University, Kumamoto 860-8556, Japan

[2]Department of Neurosurgery, Faculty of Life Sciences, Kumamoto University, Kumamoto 860-8556, Japan

[3]Center for Metabolic Regulation of Healthy Aging, Faculty of Life Sciences, Kumamoto University, Kumamoto 860-8556, Japan

[4]Department of Physiology, Okayama University Graduate School of Medicine, Dentistry and Pharmaceutical Sciences, Okayama 700-8558, Japan

[5]Neutron Therapy Research Center, Okayama University, Okayama 700-8558, Japan

[6]These authors contributed equally

*Correspondence: tomikt@kumamoto-u.ac.jp

https://doi.org/10.1016/j.isci.2019.10.012

 © 2019 The Author(s).
This is an open access article under the CC BY-NC-ND license (http://creativecommons.org/licenses/by-nc-nd/4.0/).

OXPHOS-related protein levels and triggers myopathy in mice and humans (Wei et al., 2015). Because intramitochondrial translation is a key element for sustaining malignancy and CSC-related properties, we hypothesized that CDK5RAP1 contributes to intramitochondrial translation and is essential for malignancy.

Although the importance of mitochondrial translation in malignant tumors has been emphasized, the role of CDK5RAP1 in this process is not fully understood. A previous study suggested that CDK5RAP1 deficiency induces cell-cycle arrest and apoptosis in breast cancer via the ROS/JNK signaling pathway (Wang et al., 2015). In the present study, however, we demonstrated that CDK5RAP1 deficiency induced excessive autophagy but not apoptosis and was sufficient to repress glioma-initiating cell (GIC)-related capacities. Mechanistically, CDK5RAP1 deficiency caused an intracellular accumulation of i^6A, which needs to be converted to ms^2i^6A to avoid the tumor-suppressive effects of i^6A. The results of the present study revealed a novel role of mitochondria in cancer biology, that is, a modification of mitochondrial tRNAs functions as an antidotal machinery to sustain the GIC-related traits.

RESULTS

CDK5RAP1 Is Required to Sustain GIC-Related Traits

Because GICs have been proposed to contribute to the malignant properties of glioma tissues (Lathia et al., 2015), we first examined whether CDK5RAP1 controlled the stemness of patient-derived GICs. In glioma biology, GIC-related traits are usually defined by self-renewal capacity measured using sphere formation assay, the expression of stem cell markers, and tumor-propagating potential assessed by xenograft tumor models (Suvà et al., 2014). We prepared three types of GIC cell lines categorized by their molecular subtype: JKGIC1 (mesenchymal), JKGIC2 (proneural), and JKGIC5 (proneural) (Figures S1A and S1B). Upon CDK5RAP1 knockdown by infection with lentiviruses containing shCDK5RAP1, the sphere-forming capacity of these GICs was significantly reduced (Figures 1A and S1C). Single cell-sphere formation assay showed that CDK5RAP1 was required for the *in vitro* self-renewal capacity of JKGIC2 and JKGIC5 (Figure 1B). CDK5RAP1 deficiency suppressed the protein and mRNA levels of the transcriptional factors essential for GIC (e.g., Sox2, Oig2, POU3F2, and SALL2, Suvà et al., 2014) and GIC-related markers (Figures 1C, S1D, S1F, and S1G). Immunofluorescence analyses revealed that CDK5RAP1 was required to sustain the undifferentiated state of GICs, as indicated by the loss of Sox2, Nestin, and CD133 expression in shCDK5RAP1-infected cells (Figures 1D and S1E).

We then asked whether CDK5RAP1 was required to sustain tumor-propagating capacity in subcutaneous xenograft model in immunocompromised mice (BALB/c-nu). As shown in Figure 1E, CDK5RAP1 deficit significantly reduced tumor size in all types of xenograft models. For the orthotopic glioma model, we injected JKGIC2-shControl (JKGIC2 cells infected with lentiviruses containing pLKO.1-shControl) or JKGIC2-shCDK5RAP1 (pLKO.1-shCDK5RAP1#2) cells into the left cerebral hemisphere of ICR-nu mice. The loss of CDK5RAP1 attenuated tumor growth of JKGIC2 (Figure 1F) and prolonged the overall survival of mice with brain tumors (Figure 1G). These data clearly show that CDK5RAP1 is crucial for sustaining GIC-related characteristics.

CDK5RAP1 Controls GIC Properties Independently of Mitochondrial Translation, Dynamics, and Functions

Because mitochondrial function is essential for the maintenance of GIC properties (Seyfried et al., 2015) and because CDK5RAP1 is required for the efficient translation of mitochondrial proteins encoded by mitochondrial DNA (Wei et al., 2015), we hypothesized that the loss of GIC-related traits upon CDK5RAP1 knockdown was caused by mitochondrial dysfunction, probably by a deficiency in intramitochondrial translation (Figure 2A). To test this hypothesis, we analyzed the effect of CDK5RAP1 knockdown on mitochondrial function as measured by the oxygen consumption rate (OCR) in GICs. In GICs, differentiation cues (e.g., 10% FBS) induce a regulatory switch in mitochondrial functions (Figure S2A). For this assay, we prepared three types of JKGIC2 cells: JKGIC2-shControl, JKGIC2-shCDK5RAP1#2, and JKGIC2-shCDK5RAP1#5 (the knockdown efficiency of each shRNA is shown in Figure 2B). Surprisingly, CDK5RAP1 knockdown did not affect the OCR, indicating that CDK5RAP1 is not essential for mitochondrial respiration in GICs (Figure 2B). This was specific to GICs because we observed a significant change in the OCR in shCDK5RAP1-infected U87MG cells, a non-GIC line (Figure S2B). Moreover, CDK5RAP1 deficiency did not alter mitochondrial shape or dynamics, which are considered crucial for controlling GIC-related traits (Xie et al., 2015) (Figure 2C). Electron microscopy analysis showed that there was no significant difference in the mitochondrial shape or length between control and CDK5RAP1-deficient GICs (Figure 2D).

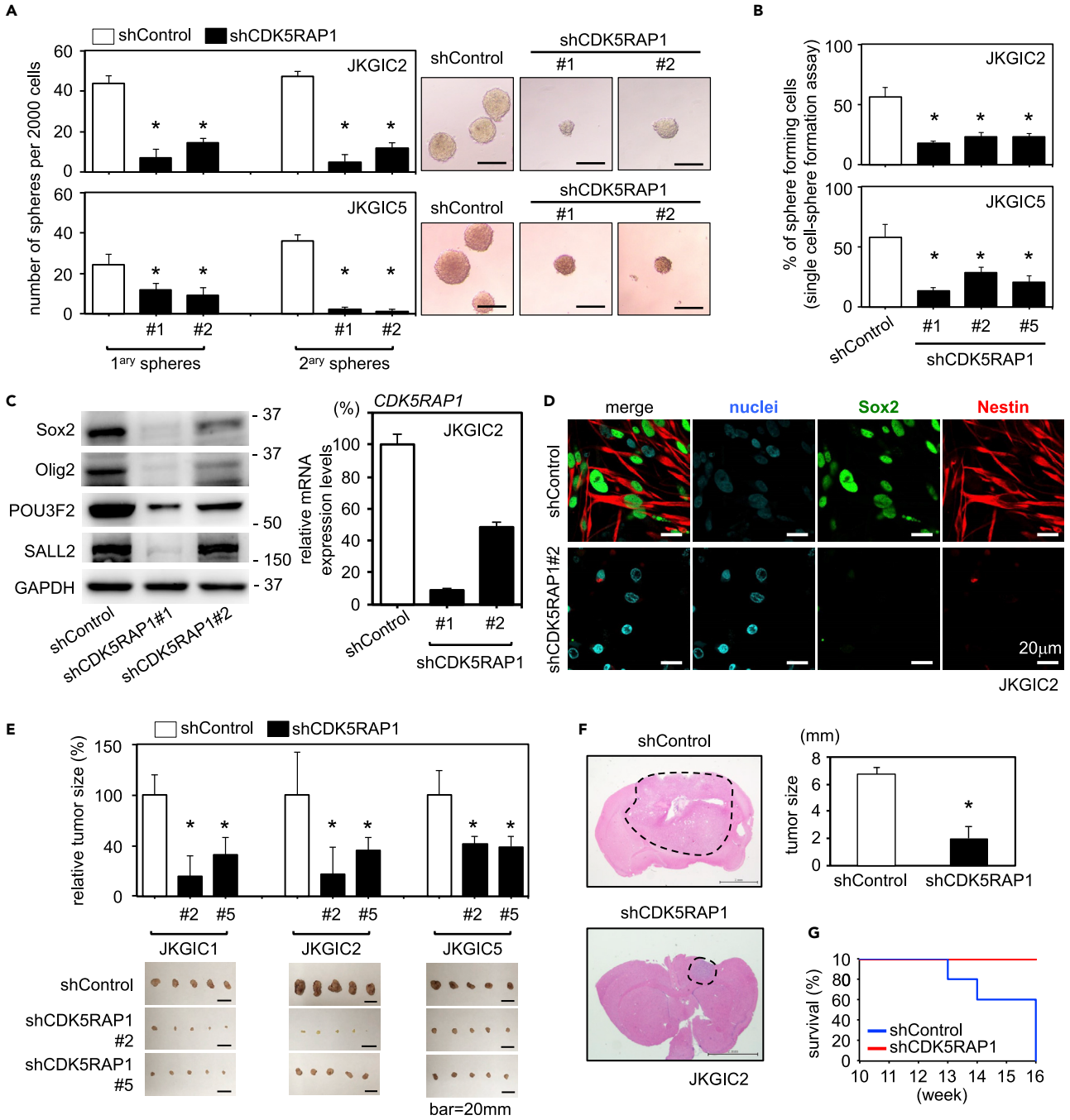

Figure 1. CDK5RAP1 Is Required to Sustain GIC-Related Traits

(A) *Left*: Quantification of primary and secondary spheres formed by JKGIC2-shControl, JKGIC2-shCDK5RAP1#1, JKGIC2-shCDK5RAP1#2 and JKGIC5-shControl, JKGIC5-shCDK5RAP1#1, JKGIC5-shCDK5RAP1#2 cells. CDK5RAP1 is required to sustain the anchorage-independent growth capacity of GICs. The data are presented as the number of spheres formed from 2,000 seeded cells. Each bar represents the SD value of four independent replicates. *p < 0.05. Sequence information of shRNAs is show in Table S1. *Right*: Representative phase contrast images of these cells. Scale bars, 100 μm.

(B) Quantification of primary spheres initiated from the single cells of JKGIC2-shControl, JKGIC2-shCDK5RAP1#1, JKGIC2-shCDK5RAP1#2, JKGIC2-shCDK5RAP1#5 and JKGIC5-shControl, JKGIC5-shCDK5RAP1#1, JKGIC5-shCDK5RAP1#2, JKGIC5-shCDK5RAP1#5. CDK5RAP1 is required for sustaining the sphere formation capacity of GICs. The data are presented as the percentage of spheres formed from 48 wells of single cells. Each bar represents the SD value of four independent replicates. *p < 0.05.

(C) *Left*: Representative immunoblotting images of GIC markers in shControl- and shCDK5RAP1-transfected JKGIC2 cells. Sox2, Olig2, POU3F2, and SALL2 levels were determined 4 days after infection with respective shRNA-encoding lentivirus. GAPDH served as a loading control. The experiment was repeated

Figure 1. *Continued*

three times. The information of antibodies used in the present study is shown in Table S2. *Right*: Relative expression levels of *CDK5RAP1* 4 days after the lentiviral transduction of shRNAs. Each bar represents the SD value from three independent replicates. Sequence information of the primers for qPCR is shown in Table S1.

(D) Representative immunostaining images of JKGIC2-shControl and JKGIC2-shCDK5RAP1 cells. Transfection with shCDK5RAP1 reduced the number of Sox2-and Nestin-positive cells. Scale bars, 20 μm.

(E–G) CDK5RAP1 is required to sustain the tumorigenic potential of GICs. After shRNA induction, JKGIC1, JKGIC2, and JKGIC5 cells were subcutaneously injected (E, n = 3 per condition) and JKGIC2 were intracranially (F, n = 5 per condition) injected. Notably, *CDK5RAP1* knockdown prolonged the overall survival of the mice with brain tumors (G). *$p < 0.05$. Scale bars: 1 cm in (E) and 2 mm in (F).

Also see Figure S1.

We then investigated whether CDK5RAP1 deficiency induced translation failure in mitochondrial proteins in GICs. As a positive control, we transduced shRNAs against the mitochondrial translation elongation factors TUFM or TSFM, which are crucial for the translation of mitochondrial proteins encoded by mitochondrial DNA (Belostotsky et al., 2012; Christian and Spremulli, 2012). In JKGIC1 cells, knockdown of TUFM or TSFM but not of CDK5RAP1 resulted in the profound loss of mitochondrially encoded cytochrome *c* oxidase I (MTCO1) (Figure 2E). Importantly, TUFM or TSFM knockdown had no effect on the sphere-forming capacity of GICs, whereas CDK5RAP1 knockdown significantly reduced the number of spheres formed (Figure 2F). We also confirmed these phenomena in JKGIC2 cells (Figures S2C and S2D). Interestingly, we noticed that CDK5RAP1 deficit reduced the level of NDUFB8 (a component of mitochondrial complex I encoded by nuclear gene) and thus induced the loss of complex I activity but did not attenuate the levels of mitochondrial proteins encoded by mitochondrial genome such as ND6, cytochrome *b*, and MTCO1 (Figures S2E and S2F). These data clearly show that intramitochondrial translation is not fundamental for sustaining GIC-related properties in glioblastoma cells and indicate that CDK5RAP1 deficiency affects the properties of GICs in an intramitochondrial translation-independent manner.

CDK5RAP1 Knockdown Induces Excessive Autophagy, which Critically Determines GIC Fate

A previous study showed that CDK5RAP1 knockdown induced cell-cycle arrest and apoptosis in breast cancer cell lines via the activation of the JNK signaling pathway (Wang et al., 2015). Therefore, we examined whether CDK5RAP1 knockdown induced apoptosis in GICs. However, CDK5RAP1 knockdown did not induce the activation of caspase 3 in JKGIC1, JKGIC2, and JKGIC5 cells (Figure 3A) and did not increase the number of TUNEL-positive cells in JKGIC2 cell lines (Figure S3A). Instead, we found that CDK5RAP1 knockdown induced autophagy as indicated by an increased presence of autophagosomes and autolysosomes in electron microscopy experiments (Figure 3B). We further validated the induction of the autophagic response in GICs upon CDK5RAP1 knockdown by immunofluorescence analysis of LC3 puncta formation and by immunoblotting analysis of LC3-II induction, AMPK activation, and mTOR inhibition (Figures 3C, 3D, S3B, and S3C).

Previous studies have demonstrated that mTOR inhibition suppresses the stemness of GICs (Garros-Regulez et al., 2016; Sunayama et al., 2010). Indeed, rapamycin treatment attenuated the cellular growth and promoted the autophagic program in GICs (Figures 3E and S3D). We then investigated whether the autophagic response triggered by CDK5RAP1 knockdown could be rescued by knocking down Atg5, which is essential for the autophagy pathway. Although Atg5 knockdown slightly reduced the number of spheres formed by JKGIC2 and JKGIC5 cells, it successfully rescued the loss of anchorage-independent growth driven by CDK5RAP1 knockdown (Figures 3F and S3E). Excessive autophagy results in the growth inhibition of GICs (Ueda et al., 2012). In agreement with our previous study, CDK5RAP1 knockdown significantly inhibited the growth of JKGIC1 and JKGIC2 cells (Figure S3F). These data demonstrate that GICs require CDK5RAP1 to avoid excessive autophagy, which critically represses the GICs' cell growth.

Treatment with N6-Isopentenyladenosine (i^6A) Induces Excessive Autophagy and Loss of GIC-Related Traits

Thus far, the present study has revealed that CDK5RAP1 maintains GIC-related traits by inhibiting excessive autophagy but not by controlling intramitochondrial translation. How does CDK5RAP1 maintain the characteristics by inhibiting excessive autophagy? CDK5RAP1 is a mitochondrial enzyme that modifies nucleosides by adding methylthio groups and is crucial for the conversion of i^6A to ms^2i^6A at A37 of mt-tRNAs (Wei et al., 2015). Consistent with this, the intracellular distribution of ms^2i^6A-containing tRNAs was limited to the mitochondria of GICs, as confirmed by immunofluorescence analysis with an anti-ms^2i^6A antibody, which specifically recognizes ms^2i^6A-containing tRNAs (Figure 4A). This result led us to hypothesize that

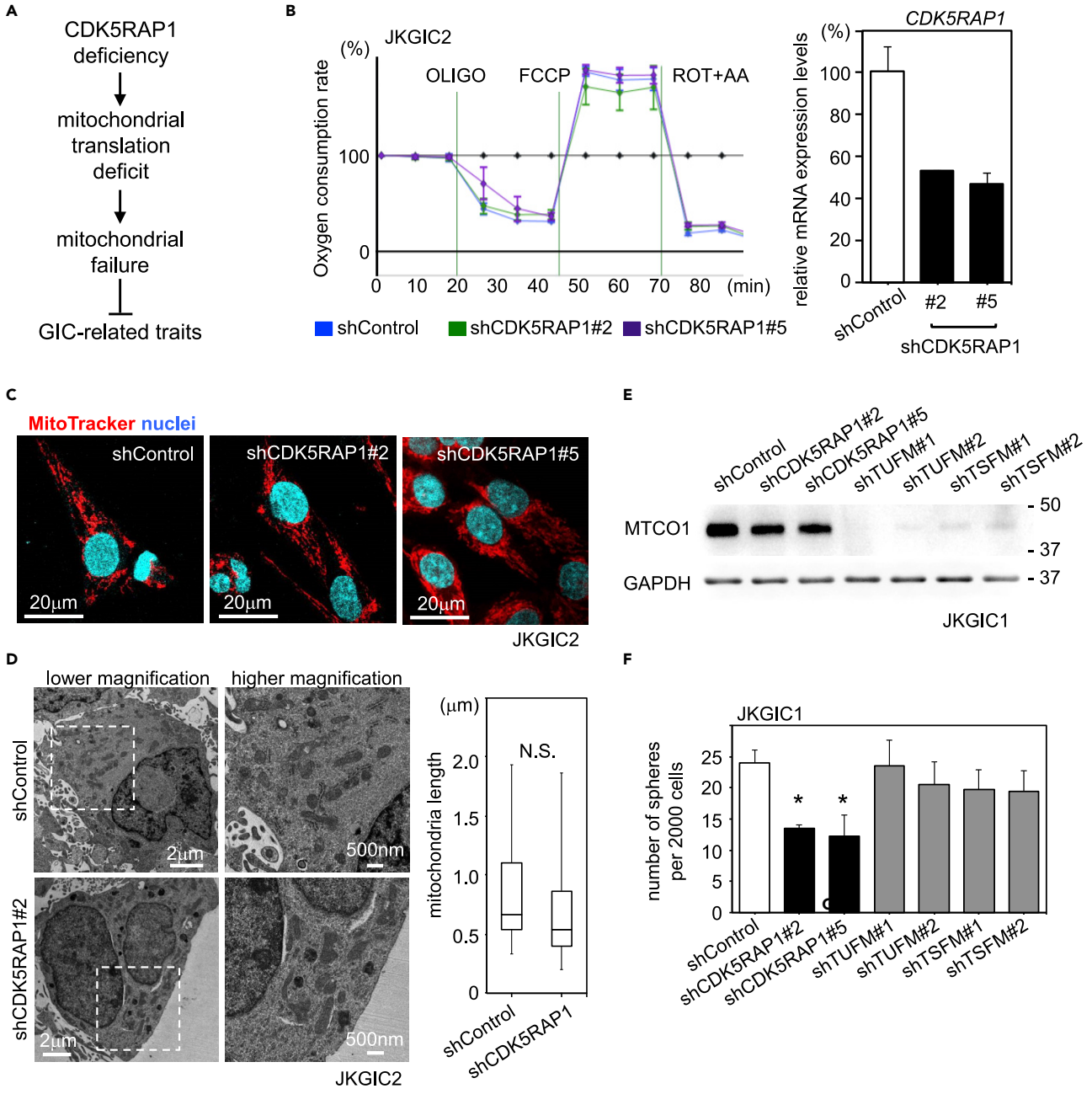

Figure 2. CDK5RAP1 Deficiency Has No Effect on Mitochondrial Translation, Dynamics, or Function

(A) An initial hypothesis suggesting that the loss of GIC-related traits by CDK5RAP1 deficiency is caused by the failure of intramitochondrial translation.

(B) *Left*: Representative oxygen consumption rates in shControl- and shCDK5RAP1-transfected JKGIC2 cells. Respiratory coupling was not affected by CDK5RAP1 knockdown. n = 5 per condition. *Right*: Relative expression levels of *CDK5RAP1* 4 days after the lentiviral transduction of shRNAs. Each bar represents the SD value from three independent replicates.

(C) MitoTracker staining shows that mitochondrial shape was not altered upon *CDK5RAP1* knockdown in JKGIC2.

(D) *Left*: Representative electron microscopy images of mitochondrial structures. Scale bars, 500 nm. *Right*: Mitochondrial length was not altered upon *CDK5RAP1* knockdown. n = 38 for shControl and n = 87 for shCDK5RAP1#2.

(E) The level of MTCO1 encoded by mitochondrial DNA was determined 4 days after shRNA lentiviral infection. GAPDH served as a loading control. The same results were reproduced three times.

(F) Quantification of primary spheres formed from 2,000 JKGIC1 cells, which were transfected with shRNAs against CDK5RAP1, TUFM, or TSFM. Only shRNAs against CDK5RAP1 reduced the number of spheres formed. Each bar represents the SD value from four independent replicates. *$p < 0.05$.

Also see Figure S2.

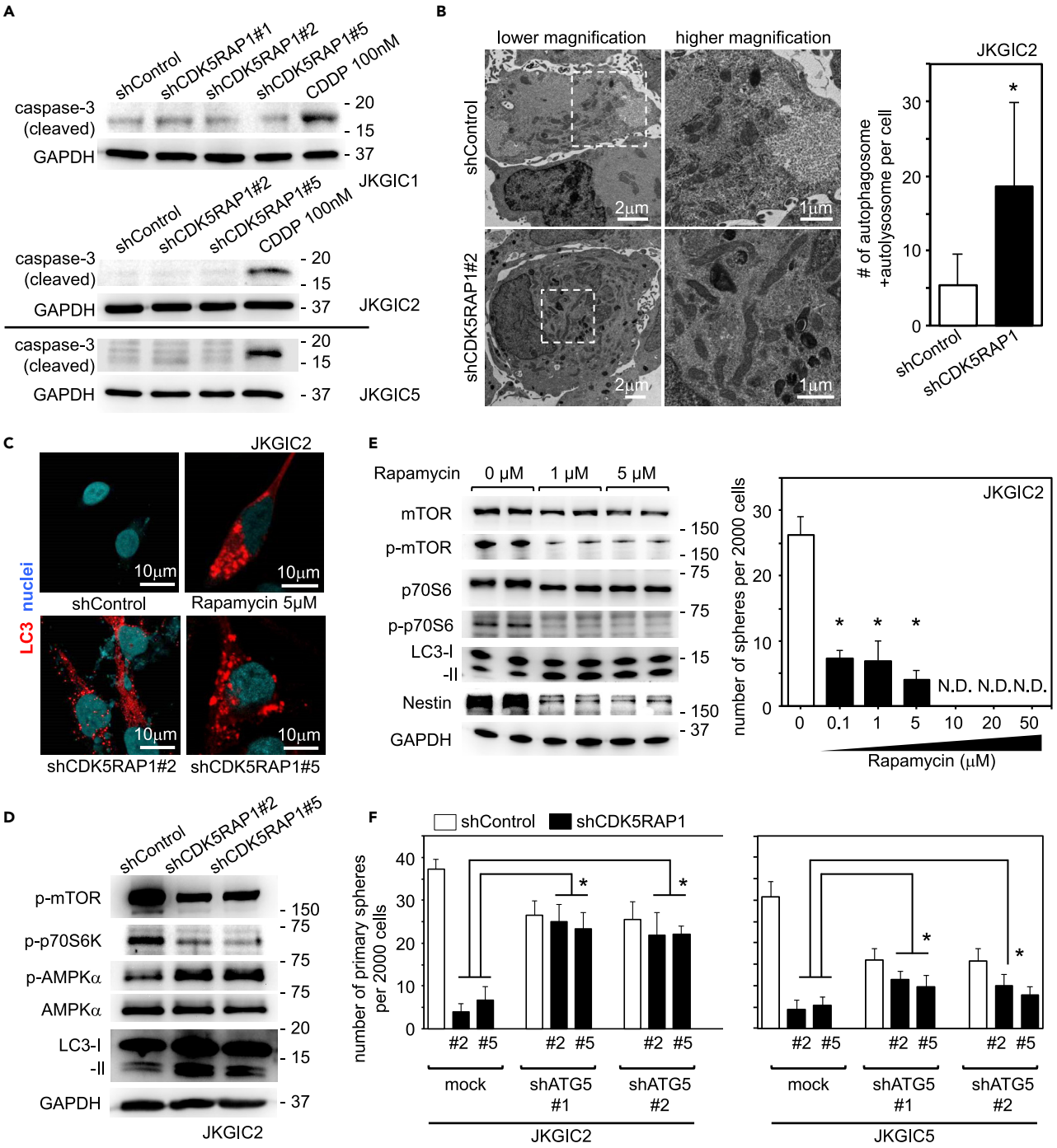

Figure 3. CDK5RAP1 Knockdown Induces Excessive Autophagy, Which Critically Determines GIC Fate

(A) CDK5RAP1 knockdown did not activate caspase-3 in JKGIC1, JKGIC2, and JKGIC5 cells. CDDP-treated cells served as a positive control of apoptotic status.

(B) *Left*: Representative electron microscopy images of the autophagic response. JKGIC2 cells were fixed after 4 days of lentiviral transduction of each shRNAs. *Right*: CDK5RAP1 knockdown increased the number of autophagosomes and autolysosomes. n = 5 per condition. *p = 0.0391 versus shControl. Scale bars, 1 μm.

(C) Representative immunostaining images for LC3 in JKGIC2 cells. CDK5RAP1 knockdown induces LC3 puncta formation. Rapamycin-treated cells served as a positive control of LC3 puncta formation. Scale bars, 10 μm.

(D) Immunoblotting analyses of mTOR, AMPK, and LC3 show that CDK5RAP1 knockdown activates the autophagic program in JKGIC2 cells.

Figure 3. *Continued*

(E) *Left*: mTOR inhibition with rapamycin triggers the autophagic response and decreases Nestin expression in JKGIC2 cells. n = 5 per condition. *Right*: Dose-dependent effect of rapamycin on the number of spheres formed from 2,000 JKGIC2 cells. Each bar represents the SD value from four independent replicates. *$p < 0.05$.

(F) Comparison of sphere formation by JKGIC2 and JKGIC5 cells transfected with shRNAs against CDK5RAP1 in the presence or absence of shRNAs against ATG5. ATG5 knockdown reduces the sphere-forming capacity but successfully rescues the shCDK5RAP1-mediated decrease in the anchorage-independent growth of GICs. Each bar represents the SD value from four independent replicates. *$p < 0.05$.

Also see Figure S3.

CDK5RAP1 enhances the conversion of i^6A to ms^2i^6A in mt-tRNAs of GICs, resulting in the inhibition of excessive autophagy.

Because previous studies have shown that treatment with exogenous i^6A induces tumor-suppressive effects such as apoptotic or autophagic cell death in cancer cells (Castiglioni et al., 2013; Ciaglia et al., 2017; Laezza et al., 2009; Rajabi et al., 2010; Ranieri et al., 2018), we examined whether i^6A treatment induced excessive autophagy and consequent loss of GIC-related traits. In JKGIC2 cells, i^6A treatment increased the intracellular concentration of i^6A in a dose-dependent manner, and the intracellular concentration of i^6A in the cells treated with 4 μM i^6A reached the same level as that in JKGIC2 cells transfected with shCDK5RAP1 (Figure S4A). However, exogenous i^6A did not induce a consequent increase in ms^2i^6A (Figure S4A), suggesting that CDK5RAP1 could not convert free i^6A to ms^2i^6A. i^6A treatment activated the autophagic program, as shown by LC3-II induction, AMPK activation, mTOR signaling pathway inhibition in JKGIC2 and JKGIC5 cells (Figures 4B, 4C, and S4B), and LC3 puncta formation in JKGIC2 cells (Figure 4D). i^6A also attenuated the anchorage-independent cell growth and reduced the expression of GIC markers such as Sox2 and Nestin (Figures 4E–4G, S4B, and S4C). To validate that the loss of GIC-related traits driven by i^6A treatment was in the context of autophagy, we prepared shControl- and shATG5-transfected JKGIC2 cells and treated them with variable concentrations of i^6A. As expected, ATG5 knockdown successfully mitigated the phenotypic outcome of i^6A (Figure 4H). In contrast, ms^2i^6A treatment induced neither autophagy nor loss of GIC-related traits and did not prevent the phenotypic outcomes triggered by i^6A treatment (Figures 4B–4G). Moreover, N6-isopentenyladenine (i^6Adenine) did not repress the anchorage-independent growth of JKGIC2 cells (Figure S4D). These data suggest that isopentenyl modification only on adenosine molecules elicits tumor-suppressive effects and that this increase in isopentenyl groups can be ameliorated via detoxification by CDK5RAP1-mediated methylthiolation (Figure S4E).

We next investigated whether the elevated expression levels of CDK5RAP1 conferred an antiautophagic phenotype to GICs. For this purpose, we transduced control red fluorescent protein (RFP) (pTomo-RFP) or murine Cdk5rap1 (pTomo-mCdk5rap1) into JKGIC2 cells (Figure 4I). Cdk5rap1 promoted the growth capacity of JKGIC2 and elevated the expression levels of the undifferentiated marker Nestin (Figures 4I and 4J). Exogenous Cdk5rap1 significantly attenuated the inhibitory effect of 3–4 μM i^6A on the anchorage-independent growth ability and cell viability of JKGIC2 cells (Figures 4K and S4F). However, overexpression of Cdk5rap1 failed to attenuate the inhibitory effect of higher concentrations (>6 μM) of exogenous i^6A (Figures 4K and S4F). Taken together, these results suggest that treatment with exogenous i^6A induces excessive autophagy and loss of GIC-related traits. Cdk5rap1 overexpression induces the conversion of endogenous i^6A to ms^2i^6A on tRNA species, resulting in a decrease in total i^6A (endogenous + exogenous i^6A) levels in GICs and consequent attenuation of the inhibitory effect of i^6A on the anchorage-independent growth ability and cell viability of GICs when treated with 3–4 μM i^6A. In contrast, when cells are treated with a high concentration (>6 μM) of i^6A, the intracellular i^6A level may reach the concentration corresponding to an antitumor effect. Therefore, the overexpression of Cdk5rap1 fails to attenuate the inhibitory effect of excessive exogenous i^6A.

CDK5RAP1 Balances i^6A and ms^2i^6A Concentrations in GICs in Response to the Microenvironment

To demonstrate whether CDK5RAP1 regulates endogenous concentrations of i^6A and ms^2i^6A in GICs, we analyzed [i^6A] and [ms^2i^6A] in mock-, shCDK5RAP1-, and mCdk5rap1-transduced JKGIC1, or JKGIC2 cells by mass spectrometry. The results showed that the ratio of total [i^6A]/[i^6A + ms^2i^6A] was increased in shCDK5RAP1-transfected cells but decreased in murine Cdk5rap1-overexpressing cells (Figures 5A and S5A).

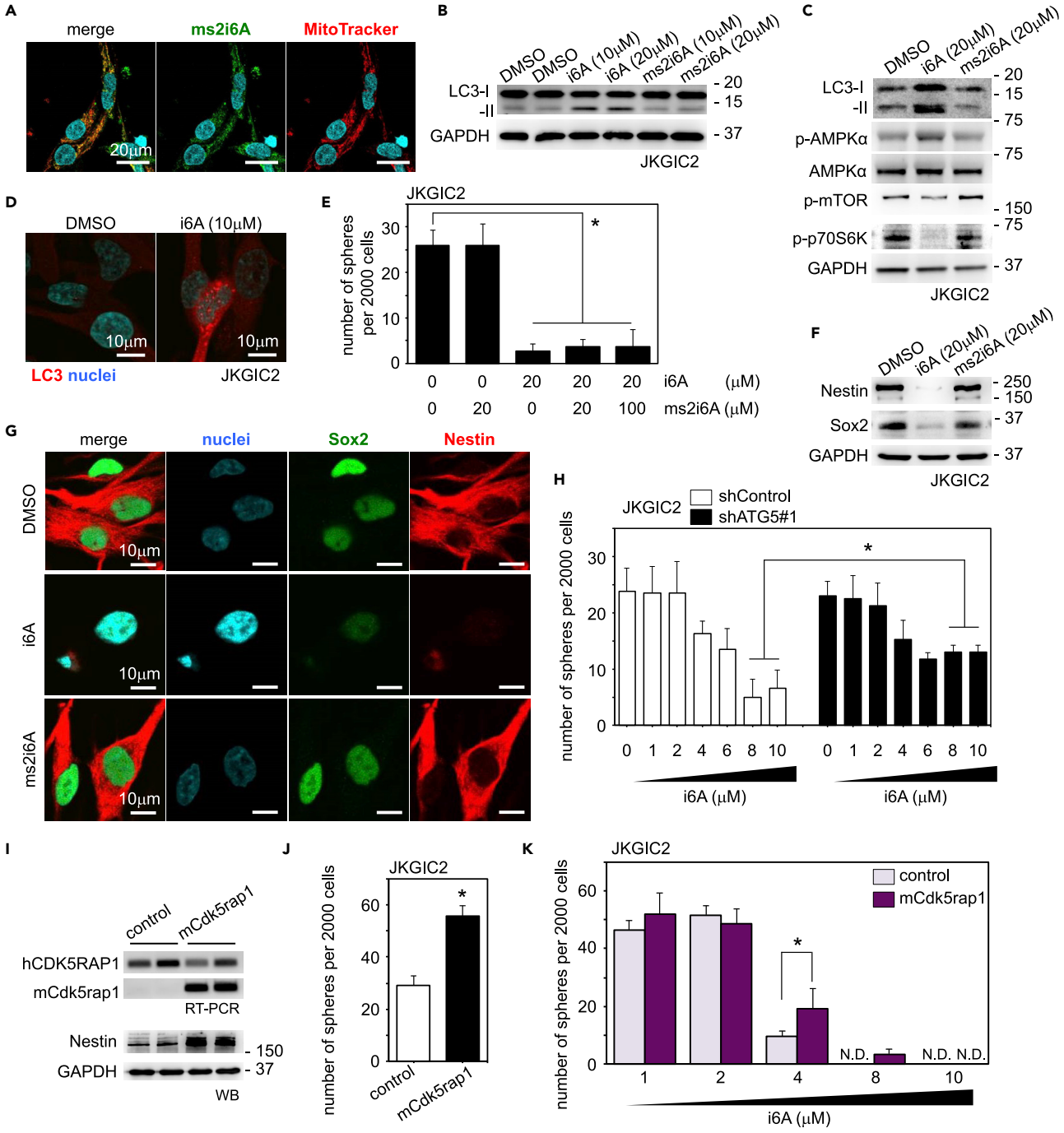

Figure 4. Treatment with N6-isopentenyladenosine (i^6A) Induces Excessive Autophagy and Loss of GIC-Related Traits

(A) Representative images of immunostaining with an anti-ms^2i^6A antibody and MitoTracker in JKGIC2 cells. Note that the intracellular distribution of ms^2i^6A is limited to the mitochondria. Scale bars, 20 μm.

(B) Treatment with i^6A, but not ms^2i^6A, for 24 h induces increases in LC3-II levels in JKGIC2 cells. GAPDH served as a loading control. The same results were reproduced three times.

(C) Treatment with i^6A, but not ms^2i^6A, activates the autophagic program in JKGIC2 cells.

(D) Treatment with i^6A for 24 h induces LC3 puncta formation in JKGIC2 cells.

(E) Quantification of primary spheres formed by JKGIC2 cells treated with i^6A or ms^2i^6A. Treatment with i^6A reduces the number of spheres, but this reduction is not rescued by the further addition of ms^2i^6A. Each bar represents the SD value from four independent replicates. *$p < 0.05$.

(F and G) Immunoblotting (F) and immunostaining (G) indicate that treatment with i^6A, but not ms^2i^6A, decreases the protein levels of Nestin and Sox2 in JKGIC2 cells.

Figure 4. *Continued*

(H) Quantification of primary spheres formed by JKGIC2 cells (2,000/well) transfected with shRNAs against ATG5 and i^6A. ATG5 knockdown successfully rescues the i^6A-induced loss of stemness in JKGIC2 cells. Each bar represents the SD value from four independent replicates. *: $p < 0.05$.

(I and J) Exogenous transduction of murine Cdk5rap1 increases the amount of Nestin protein (I) and the number of spheres formed by JKGIC2 cells (2,000/well) (J). Each bar represents the SD value from four independent replicates. *$p < 0.05$.

(K) Ectopic expression of murine Cdk5rap1 prevents the loss of anchorage-independent growth ability in JKGIC2 due to exogenous treatment with 4 and 8 μM i^6A. The data are presented as the number of spheres formed from 2,000 cells. Each bar represents the SD value from four independent replicates. *$p < 0.05$.

Also see Figure S4.

Because the biochemical reaction of CDK5RAP1-mediated 2-methylthio conversion of i^6A is strictly regulated within the mitochondria and is detected solely in mt-tRNAs (Fakruddin et al., 2017) and because ms^2i^6A is predominantly enriched in cell culture medium (~9.6 times more than the concentration inside cells, Figure S5B), these data suggest that CDK5RAP1 decreases [i^6A] by promoting the 2-methylthio conversion of i^6A in the mitochondria and that the consequent ms^2i^6A derived from degraded mt-tRNAs is excreted (Figure S5C).

Two conserved domains in CDK5RAP1, namely, UPF0004 and the radical SAM domain, are essential for CDK5RAP1 activity (Fakruddin et al., 2017). The cysteine residues in these domains are required for the interaction with both [4Fe-4S] clusters, which provide the sulfur atoms for interactions with i^6A molecules (Figure 5B). Given that [4Fe-4S] clusters are stable under anoxic conditions (Crack et al., 2007), we speculated that CDK5RAP1 was activated under hypoxic conditions. To test this possibility, we performed quantitative PCR measurements of tRNA 2-methylthio modifications. We extracted total RNA from GICs cultured in the presence of either 21% or 1% O_2. The ms^2i^6A modifications in each mt-tRNA are represented as a modification index (M.I.) as reported previously (Figure S5D) (Xie et al., 2013). As expected, hypoxic culture conditions significantly increased the M.I. of each CDK5RAP1-targeted mt-tRNA, whereas hypoxic conditions had no effect on the expression of the tRNAs (Figures 5C and S5E). Consistent with this outcome, as observed in mCdk5rap1-overexpressing JKGIC1 and JKGIC2 cells, the ratio of total [i^6A]/[i^6A + ms^2i^6A] under hypoxic conditions was decreased, whereas the ratio of [ms^2i^6A]/[i^6A + ms^2i^6A] was increased (Figures 5D and S5F). Hypoxia-inducible factor 1α (HIF-1α) is the inducible subunit of the HIF-1 transcription factor that regulates the expression of genes involved in the response to hypoxia. Vascular endothelial growth factor (VEGF) is one of the genes upregulated by HIF-1 (Lin et al., 2004). *VEGF* expression was significantly increased in GICs cells cultured under 1% O_2 (Figures 5E, S5G, and S5I). In contrast, there was no difference in the expression level of *CDK5RAP1* in cells cultured in the presence of 21% to 1% O_2 (Figures 5F, S5H, and S5J). To further validate that [4Fe-4S] clusters are required for this reaction, we treated cells with deferoxamine (100 μM) to chelate intracellular Fe ions and measured the M.I. of the mt-tRNAs, and we found that Fe chelation reduced the M.I (Figure S5K). These data indicate that CDK5RAP1 activity is controlled by the microenvironment, such as hypoxic conditions and the concentration of intracellular Fe ions.

CDK5RAP1 Activity Is Upregulated in the Hypoxic Region of Human Glioblastoma and Is Required to Sustain the Sphere-forming Capacity of Malignant Cells but Not Normal Brain Cells

To gain insights into the contribution of CDK5RAP1 to human glioblastoma multiforme (GBM) pathophysiology, we harvested several specimens, including the "tumor core" and "peritumor normal area," from three patients with GBM and analyzed the concentrations of i^6A and ms^2i^6A by mass spectrometry. Intriguingly, [i^6A] was significantly increased in the tumor core compared with that in the peritumor normal area in all cases (Figure 6A). Following the logic established by these observations and the above-mentioned data, we hypothesized that glioblastoma cells require CDK5RAP1 activity to detoxify i^6A to protect cells from excessive autophagy. However, the expression level of CDK5RAP1 in the tumor core was the same as that in the peritumor normal area (Figure 6B). Because the GBM core is known to be hypoxic (Fujimura et al., 2013), we speculated that CDK5RAP1 activity was upregulated in the tumor core of GBM specimens. RT-PCR analysis of a HIF target gene, *VEGF*, indicated that the tumor core was more hypoxic than the peritumor normal area (Figure 6C). As expected, mass spectrometry analysis showed that [ms^2i^6A] in the tumor core was higher than that in the peritumor normal area (Figure 6D). Immunofluorescence analysis revealed that Nestin-positive tumor cells overlapped with ms^2i^6A-positive tumor cells in the tumor core area, whereas ms^2i^6A-negative tumor cells did not overlap with Nestin-positive cells (Figure 6E), suggesting

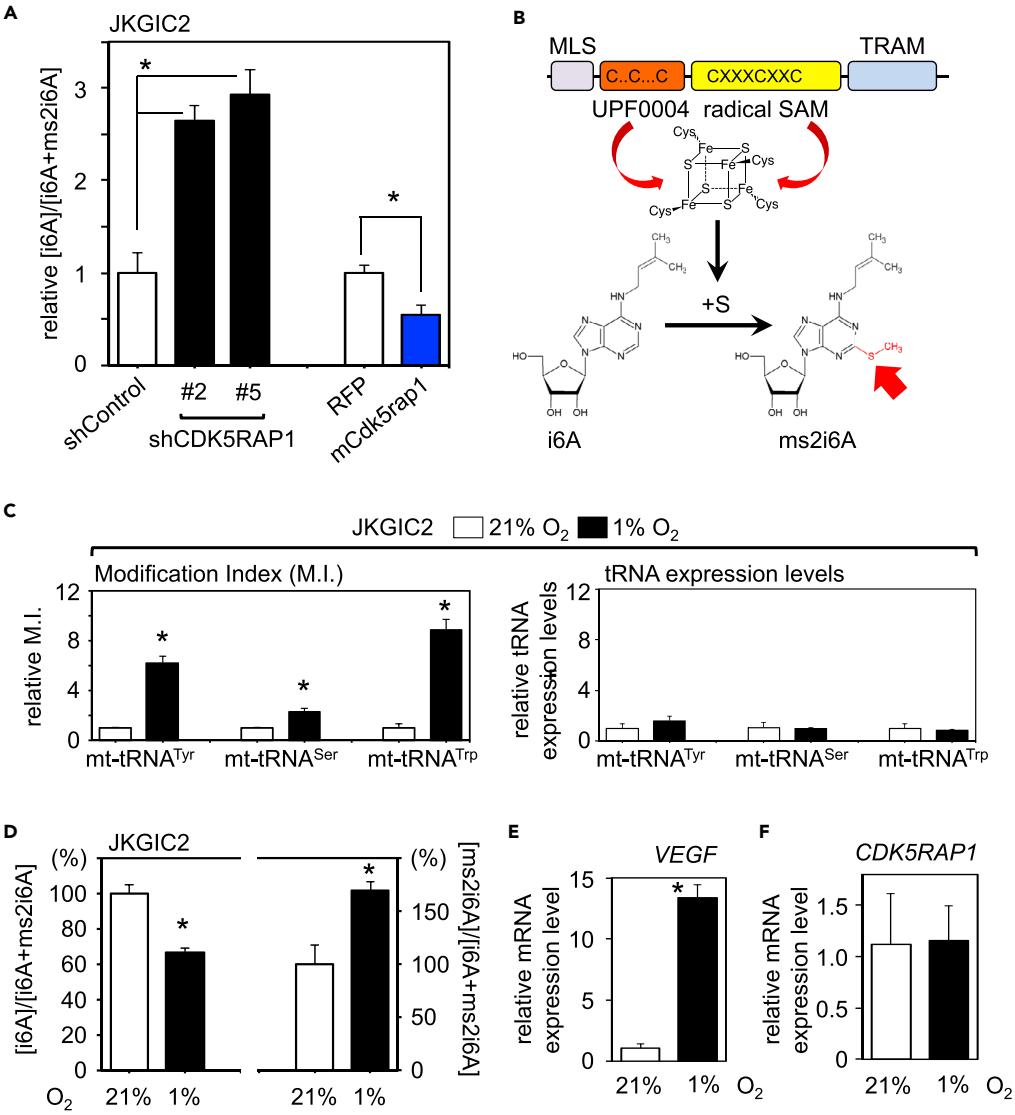

Figure 5. CDK5RAP1 Balances i^6A and ms^2i^6A Concentrations in GICs in Response to the Microenvironment

(A) Mass spectrometry analysis of [i^6A] and [ms^2i^6A] from the lysates of shControl- and shCDK5RAP1-, RFP-, mCdk5rap1-transfected JKGIC2 cells. Note that CDK5RAP1 knockdown induces an increase in the relative [i^6A] in GICs, whereas CDK5RAP1 overexpression reduces the relative [i^6A]. Each bar represents the SD value from three independent replicates. *$p < 0.05$.

(B) Schematic representation of the molecular characteristics of CDK5RAP1. Cysteine residues in the UPF0004 and radical SAM domains are crucial for the stabilization of the [4Fe-4S] clusters. The mitochondria localization signal (MLS) allows CDK5RAP1 to localize to the mitochondria. The TRAM domain is predicted to interact with tRNA species.

(C) The M.I. of ms^2i^6A corresponding to each mt-tRNA and tRNA expression level in JKGIC2 cells cultured in the presence of 21% and 1% O_2. The M.I.s in all CDK5RAP1-targeted tRNA species are increased under hypoxic conditions, but tRNA expression is not. The data are presented as the M.I. relative to the cells cultured under normoxia. Each bar represents the SD value from two independent replicates. For the procedure regarding the measurement of M.I., also see Figure S5D.

(D) Hypoxic conditions decrease intracellular [i^6A] and increase the secretion of ms^2i^6A by JKGIC2 cells. The data are presented as the percentage of the levels under normoxia. Each bar represents the SD value from three independent replicates. *$p < 0.05$.

(E and F) Hypoxic conditions significantly increased the expression levels of *VEGF* mRNA (E) but not *CDK5RAP1* mRNA (F) in JKGIC2 cells. Each bar represents the SD value from four independent replicates. *$p < 0.05$.

Also see Figure S5.

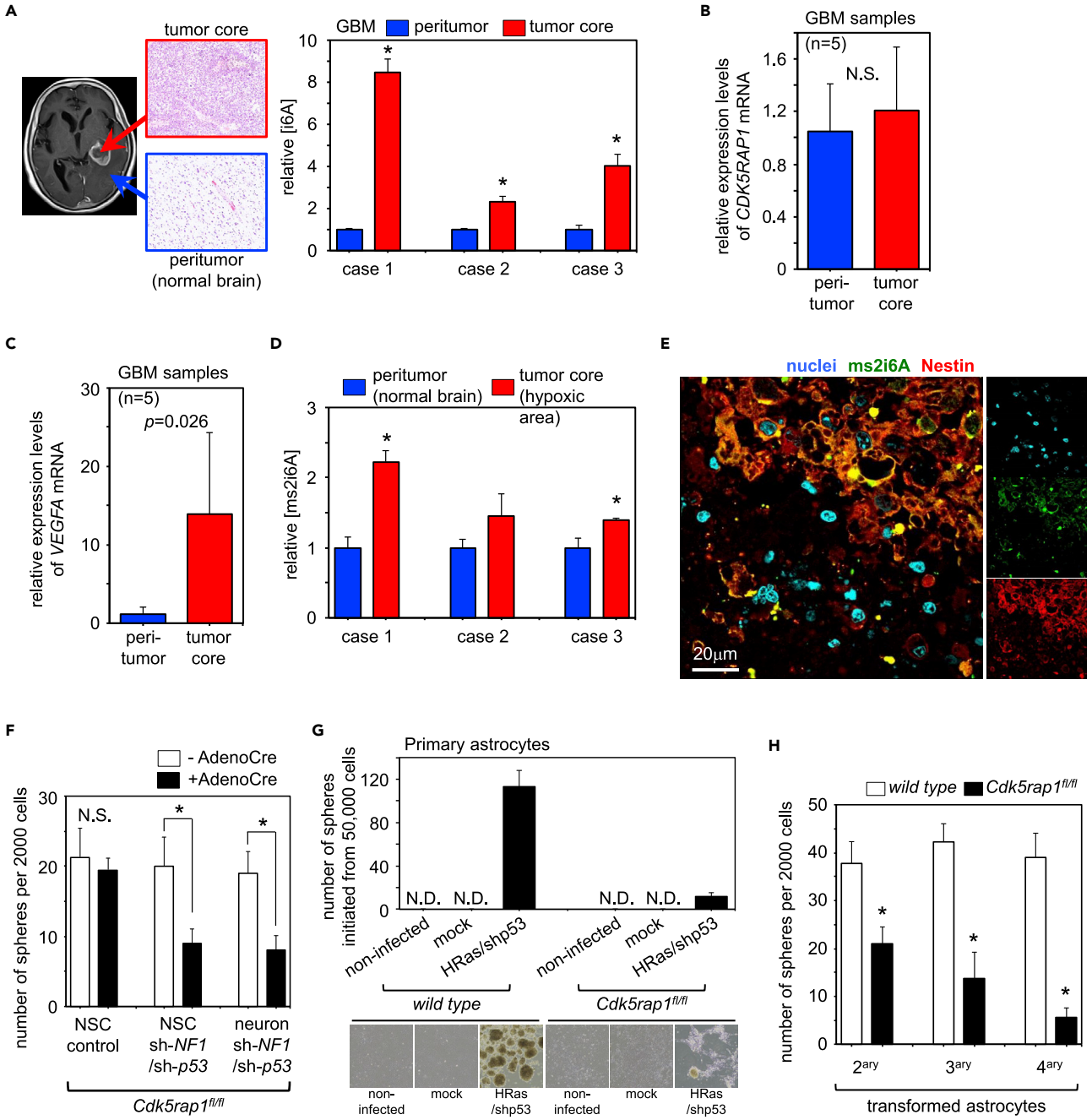

Figure 6. CDK5RAP1 Is Essential for Sustaining the GIC-Related Traits of GICs but Not That of Normal Brain Cells

(A) *Left*: Representative MR image and H&E staining of the brain tissue in a patient (case 1) with GBM. Tumor core and peritumor samples were harvested to extract RNA and nucleosides. *Right*: Mass spectrometry analysis of relative [i^{6}A] shows that [i^{6}A] is increased in the tumor core. Each bar represents the SD value from three independent replicates. *p < 0.05 versus the peritumor sample.

(B) Expression levels of *CDK5RAP1* in human GBM specimens from the tumor core and peritumor areas are not significantly different. n = 5 per sample type.

(C) Expression level of *VEGF* in the peritumor and tumor core areas of patients with GBM. n = 5 per sample type.

(D) Mass spectrometry analysis of relative [ms^{2}i^{6}A] in the peritumor and tumor core areas of specimens from patients with GBM. Each bar represents the SD value from three independent replicates. *p < 0.05 versus the peritumor sample.

(E) Representative images of immunofluorescence analysis with anti-ms^{2}i^{6}A and anti-Nestin antibodies in the tumor core of patients with GBM. Note that the ms^{2}i^{6}A-positive cells and Nestin-positive cells overlap.

(F) Untreated NSCs, NSCs transformed with oncogenic lentiviruses, and mouse primary neurons transformed with oncogenic lentiviruses (all from *Cdk5rap1*$^{fl/fl}$ mouse brains) either with or without transduced adenoviruses harboring Cre recombinase were subjected to the sphere formation assay.

Figure 6. *Continued*

Transformed cells but not NSCs require Cdk5rap1 to sustain their anchorage-independent growth capacity. The data are presented as the number of spheres formed from 2,000 cells. Each bar represents the SD value from four independent replicates. *$p < 0.05$.

(G) Representative data of the gliosphere initiation assay. Primary astrocytes from *wild-type* or *Cdk5rap1*$^{fl/fl}$ mouse brains were infected with Cre-inducible HRas^{G12V}-expressing pTomo lentiviruses. The cells were further infected with adenoviruses harboring Cre recombinase to activate HRas^{G12V} and recombine out the *Cdk5rap1* alleles and were cultured in GIC medium for 7–10 days. The numbers of initiated spheres from 50,000 cells were counted. n = 4 per condition. For the procedure of the gliosphere initiation assay, see Figure S6. Cdk5rap1 is required to initiate the formation of gliospheres from primary astrocytes.

(H) Quantification of secondary, tertiary, and quaternary spheres formed by the transformed astrocytes harvested from the gliosphere initiation assay described in (G). Cdk5rap1 is required to sustain the self-renewal capacity of the transformed cells. The data are presented as the number of spheres formed from 2,000 cells. Each bar represents the SD value from four independent replicates. *$p < 0.05$.

Also see Figure S6.

that CDK5RAP1, upon activation under hypoxic conditions, promotes the maintenance of GIC-related traits.

To demonstrate whether CDK5RAP1 activity was required for the traits of only GICs but not normal neural stem cells (NSCs), we prepared NSCs and primary neurons from *Cdk5rap1*$^{fl/fl}$ mouse pups and infected these cells with control pTomo lentivirus or pTomo-shNF1-shp53 lentivirus. Dual knockdown of *NF1* and *p53* allowed the neural cells to acquire GIC-related properties within 1–2 weeks as previously reported (Friedmann-Morvinski et al., 2012). After several passages, we further infected the cells with adenoviruses harboring Cre recombinase to knockout the *Cdk5rap1* alleles from these cells, after which the cells were subjected to the sphere formation assay. The *Cdk5rap1* knockout resulted in a significant reduction of the anchorage-independent growth in the transformed NSCs and neurons, but not in normal NSCs (Figure 6F). We further investigated whether Cdk5rap1 was required for the acquisition of GIC-related traits (i.e., gliomagenesis). We transduced Cre-inducible HRas^{G12V}/shp53 into astrocytes from wild-type and *Cdk5rap1*$^{fl/fl}$ mouse pups. The infected cells were subjected to sphere formation assays upon adeno-Cre infection, which further recombined out the loxP-RFP-loxP cassette to induce HRas^{G12V} expression (Figure S6). In the astrocytes from *Cdk5rap1*$^{fl/fl}$ mice, adeno-Cre infection recombined the *Cdk5rap1* alleles out. Using the gliosphere initiation assay, we found that wild-type astrocytes with *HRas* induction and *p53* knockdown (HRas/shp53) formed numerous spheres, suggesting that the primary astrocytes acquired GIC-related properties. In contrast, the number of spheres in primary astrocytes from *Cdk5rap1*$^{fl/fl}$ mice was lower than that in HRas/shp53 astrocytes, suggesting that astrocytes required Cdk5rap1 to achieve gliomagenesis (Figure 6G). We then harvested and trypsinized the formed spheres and conducted the sphere formation assay. Similar to the transformed neurons, the anchorage-independent growth of the cells was reduced upon *Cdk5rap1* deletion (Figure 6H). These data clearly demonstrate that CDK5RAP1 is essential for acquiring and sustaining the GIC-related traits of malignant and transformed cells but not that of normal NSCs.

DISCUSSION

We previously reported that CDK5RAP1 was responsible for the ms^2 modification of mammalian mt-tRNAs for the Ser (UCN), Phe, Tyr, and Trp codons (Wei et al., 2015). Under stress condition, deficiencies in ms^2 modification impaired mitochondrial protein synthesis, OXPHOS activity, and ATP synthesis in normal tissues. Although the canonical role of CDK5RAP1 is to regulate the precise translation of mitochondrial DNA-encoded genes, even in the knockout mice the effect of loss-of-CDK5RAP1 can be observed mainly in complex I but not markedly in the other complexes in steady state (Wei et al., 2015). In the present study, we demonstrate that CDK5RAP1 deficiency induces excessive autophagy and the consequent loss of GIC-related traits. Importantly, we reveal that these phenomena are independent from the regulation of intramitochondrial translation by CDK5RAP1 in GICs, and moreover, we show that the intramitochondrial translation seems not to contribute to sustain the GIC-related traits (Figures 2 and S2). In GICs, CDK5RAP1 deficiency attenuates the antidotal effect of ms^{2}i^{6}A against i^{6}A in the mitochondria, resulting in the promotion of tumor-suppressive effects of i^{6}A. The present study suggests a novel function of CDK5RAP1-mediated ms^2 modification corresponding to the detoxification of i^{6}A in the mitochondria; GICs readily exploit this function to survive. We propose mitochondria as the sole antidotal machinery against i^{6}A, which causes excessive autophagy and the consequent loss of GIC-related traits. The data presented here add a new layer of the function of chemical modification in mitochondrial tRNAs.

The present study showed that CDK5RAP1 was essential for acquiring and sustaining the GIC-related traits of malignant and transformed cells but not that of normal NSCs by the conversion of i^6A to ms^2i^6A. A recent study showed lower proliferation and differentiation capabilities in NSCs in an adult rodent model of severe motor deprivation and a significant reduction in *Cdk5rap1* expression in NSCs in the model (Adami et al., 2018). Although it is unclear that a reduction in *Cdk5rap1* expression impairs proliferation and differentiation capabilities in NSCs, the canonical function and the regulation of precise translation of the mitochondrial protein may be involved in the proliferation and differentiation of NSCs. Thus, the functions of CDK5RAP1 may differ between NSCs and GICs.

In glioblastoma specimens, i^6A was enriched in the tumor core area. Consistent with this, the expression levels of TRIT1, a mitochondrial tRNA isopentenyl transferase, were elevated in malignant tissues from the REMBRANDT cohort (REpository for Molecular BRAin Neoplasia DaTa, http://www.betastasis.com/glioma/rembrandt/). Such environmental conditions can promote excessive autophagy in GICs and consequently repress GIC-related properties, as demonstrated by the present study. To survive in this microenvironment, GICs require robust CDK5RAP1 activity. However, the expression of *CDK5RAP1* in the tumor core was the same as that in the peritumoral normal area. Therefore, it may be important for GICs to survive under hypoxic conditions, such as those in the tumor core, to activate CDK5RAP1. CDK5RAP1 has two [4Fe-4S] clusters, which are essential for its enzymatic activity and are sensitive to oxygen (Wei et al., 2015). As shown in the present study, the activity of CDK5RAP1 was drastically increased under hypoxic conditions, although its expression was not induced under these conditions (Figures 5C–5F). The hypoxic area is known to harbor a subset of cells, known as CSCs, that have stem cell-like properties due to the induction of stemness genes such as Oct4, c-myc, and Nanog. Moreover, hypoxia induces drug resistance in GICs by activating several pathways mediated by COX-2, the PI3K pathway, AP1, c-Jun, Pim1, or Stat3 (Jalota et al., 2018). Our findings suggest a novel importance of the hypoxic environment for the survival and maintenance of GIC-related traits. Thus, GICs likely require continuous activation of CDK5RAP1.

The results of the present study show that CDK5RAP1 deficiency induces excessive autophagy and the consequent loss of stemness in GICs but not in normal neurons or NSCs. The Warburg effect is a metabolic phenomenon characterized by increased glycolytic activity, decreased mitochondrial oxidative phosphorylation, and lactate production and is often observed in GICs (Koppenol et al., 2011). Functional differences in CDK5RAP1 between normal cells and GICs may be due to the difference in the metabolic phenotypes of the mitochondria in the cells.

A number of studies have shown that exogenous application of i^6A has a strong antitumor effect *in vitro* (Castiglioni et al., 2013; Ciaglia et al., 2017; Laezza et al., 2009; Rajabi et al., 2010; Ranieri et al., 2018). In agreement with previous studies, the present study showed that i^6A inhibited the GIC-related traits and induced autophagic cell death and that exogenous i^6A was not converted to ms^2i^6A by CDK5RAP1. These results suggest that i^6A is a promising therapeutic molecule to target GICs. However, a higher concentration (>4 μM) of exogenous i^6A was required for the antitumor effect against GICs. The effective concentration of exogenous i^6A seems to be much higher than endogenous i^6A produced from degraded tRNAs. Importantly, the level of intracellular i^6A when treated with 4 μM i^6A was consistent with that in shCDK5RAP1-transfected JKGIC2 cells (Figure S4A). These results suggest that the membrane permeability of i^6A is poor and/or that exogenous i^6A is rapidly excreted after entering GICs. It may be important for clinical applications to develop delivery systems that can effectively deliver and maintain i^6A in GICs. Moreover, i^6A was significantly enriched in the tumor core where GICs are abundant, suggesting that i^6A alone may be ineffective in combating GICs in the hypoxic tumor core that have constitutively active CDK5RAP1. Despite the antitumor effect of i^6A *in vitro*, few studies have shown this effect *in vivo*. It may be important to combine i^6A administration with CDK5RAP1 downregulation by either an iron chelator or shRNAs against CDK5RAP1.

In conclusion, CDK5RAP1-mediated modification of mitochondrial tRNAs is crucial for not only the precise translation of mitochondrial DNA-encoded proteins in normal tissues but also the detoxification of endogenous i^6A in GICs. GICs readily utilize this mechanism to survive.

Limitations of the Study

In this study, we were unable to generate CDK5RAP1 knockout GICs because the cells could not grow. Therefore, we used the knockdown cells in all experiments.

METHODS

All methods can be found in the accompanying Transparent Methods supplemental file.

SUPPLEMENTAL INFORMATION

Supplemental Information can be found online at https://doi.org/10.1016/j.isci.2019.10.012.

ACKNOWLEDGMENTS

We thank Nobuko Maeda, Masayo Obata (Kumamoto University), and Masumi Furutani (Okayama University) for their technical assistance. This work was supported by a Grant-in-Aid for Scientific Research from the Ministry of Education, Culture, Sports, Sciences, and Technology of Japan (17905074 and 18959602 to K.T., 16K18989 and 18K15241 to A.F.), the Japan Agency for Medical Research and Development (AMED) (17935694 to K.T., JP18cm0106143 to A.F.), and the Takeda Science Foundation (K.T.).

AUTHOR CONTRIBUTIONS

T.Y., A.F., F.-Y.W., and K.T. designed the experiments and wrote the manuscript. T.Y. and A.F. carried out the experiments. N.S., J.K. and A.M. provided GBM samples.

DECLARATION OF INTERESTS

The authors declare no conflict of interest.

Received: November 22, 2018
Revised: June 4, 2019
Accepted: October 2, 2019
Published: November 22, 2019

REFERENCES

Adami, R., Pagano, J., Colombo, M., Platonova, N., Recchia, D., Chiaramonte, R., Bottinelli, R., Canepari, M., and Bottai, D. (2018). Reduction of movement in neurological diseases: effects on neural stem cells characteristics. Front. Neurosci. *12*, 336.

Belostotsky, R., Frishberg, Y., and Entelis, N. (2012). Human mitochondrial tRNA quality control in health and disease: a channelling mechanism? RNA Biol. *9*, 33–39.

Brien, G.L., Valerio, D.G., and Armstrong, S.A. (2016). Exploiting the epigenome to control cancer-promoting gene-expression programs. Cancer Cell *29*, 464–476.

Castiglioni, S., Casati, S., Ottria, R., Ciuffreda, P., and Maier, J.A. (2013). N6-isopentenyladenosine and its analogue N6-benzyladenosine induce cell cycle arrest and apoptosis in bladder carcinoma T24 cells. Anticancer Agents Med. Chem. *13*, 672–678.

Christian, B.E., and Spremulli, L.L. (2012). Mechanism of protein biosynthesis in mammalian mitochondria. Biochim. Biophys. Acta *1819*, 1035–1054.

Ciaglia, E., Abate, M., Laezza, C., Pisanti, S., Vitale, M., Seneca, V., Torelli, G., Franceschelli, S., Catapano, G., Gazzerro, P., and Bifulco, M. (2017). Antiglioma effects of N6-isopentenyladenosine, an endogenous isoprenoid end product, through the downregulation of epidermal growth factor receptor. Int. J. Cancer *140*, 959–972.

Cogliati, S., Enriquez, J.A., and Scorrano, L. (2016). Mitochondrial cristae: where beauty meets functionality. Trends Biochem. Sci. *41*, 261–273.

Crack, J.C., Green, J., Cheesman, M.R., Le Brun, N.E., and Thomson, A.J. (2007). Superoxide-mediated amplification of the oxygen-induced switch from [4Fe-4S] to [2Fe-2S] clusters in the transcriptional regulator FNR. Proc. Natl. Acad. Sci. U S A *104*, 2092–2097.

Fakruddin, M., Wei, F.Y., Emura, S., Matsuda, S., Yasukawa, T., Kang, D., and Tomizawa, K. (2017). Cdk5rap1-mediated 2-methylthio-N6-isopentenyladenosine modification is absent from nuclear-derived RNA species. Nucleic Acids Res. *45*, 11954–11961.

Friedmann-Morvinski, D., Bushong, E.A., Ke, E., Soda, Y., Marumoto, T., Singer, O., Ellisman, M.H., and Verma, I.M. (2012). Dedifferentiation of neurons and astrocytes by oncogenes can induce gliomas in mice. Science *338*, 1080–1084.

Fujimura, A., Michiue, H., Cheng, Y., Uneda, A., Tani, Y., Nishiki, T., Ichikawa, T., Wei, F.Y., Tomizawa, K., and Matsui, H. (2013). Cyclin G2 promotes hypoxia-driven local invasion of glioblastoma by orchestrating cytoskeletal dynamics. Neoplasia *15*, 1272–1281.

Garros-Regulez, L., Aldaz, P., Arrizabalaga, O., Moncho-Amor, V., Carrasco-Garcia, E., Manterola, L., Moreno-Cugnon, L., Barrena, C., Villanua, J., Ruiz, I., et al. (2016). mTOR inhibition decreases SOX2-SOX9 mediated glioma stem cell activity and temozolomide resistance. Expert Opin. Ther. Targets *20*, 393–405.

Guha, M., Srinivasan, S., Ruthel, G., Kashina, A.K., Carstens, R.P., Mendoza, A., Khanna, C., van Winkle, T., and Avadhani, N.G. (2014). Mitochondrial retrograde signaling induces epithelial-mesenchymal transition and generates breast cancer stem cells. Oncogene *33*, 5238–5250.

Jalota, A., Kumar, M., Das, B.C., Yadav, A.K., Chosdol, K., and Sinha, S. (2018). A drug combination targeting hypoxia induced chemoresistance and stemness in glioma cells. Oncotarget *9*, 18351–18366.

Koppenol, W.H., Bounds, P.L., and Dang, C.V. (2011). Otto Warburg's contributions to current concepts of cancer metabolism. Nat. Rev. Cancer *11*, 325–337.

Lacadie, S.A., Ibrahim, M.M., and Gokhale, S.A. (2016). Divergent transcription and epigenetic directionality of human promoters. FEBS J. *283*, 4214–4222.

Laezza, C., Caruso, M.G., Gentile, T., Notarnicola, M., Malfitano, A.M., Di Matola, T., Messa, C., Gazzerro, P., and Bifulco, M. (2009). N6-isopentenyladenosine inhibits cell proliferation and induces apoptosis in a human colon cancer cell line DLD1. Int. J. Cancer *124*, 1322–1329.

Lathia, J.D., Mack, S.C., Mulkearns-Hubert, E.E., Valentim, C.L.L., and Rich, J.N. (2015). Cancer stem cells in glioblastoma. Genes Dev. *29*, 1203–1217.

Lin, C., McGough, R., Aswad, B., Block, J.A., and Terek, R. (2004). Hypoxia induces HIF-1alpha and

VEGF expression in chondrosarcoma cells and chondrocytes. J. Orthop. Res. *22*, 1175–1181.

Pernas, L., and Scorrano, L. (2016). Mito-morphosis: mitochondrial fusion, fission, and cristae remodeling as key mediators of cellular function. Annu. Rev. Physiol. *78*, 505–531.

Rajabi, M., Signorelli, P., Gorincioi, E., Ghidoni, R., and Santaniello, E. (2010). Antiproliferative activity of N6-isopentenyladenosine on MCF-7 breast cancer cells: cell cycle analysis and DNA-binding study. DNA Cell Biol. *29*, 687–691.

Ranieri, R., Ciaglia, E., Amodio, G., Picardi, P., Proto, M.C., Gazzerro, P., Laezza, C., Remondelli, P., Bifulco, M., and Pisanti, S. (2018). N6-isopentenyladenosine dual targeting of AMPK and Rab7 prenylation inhibits melanoma growth through the impairment of autophagic flux. Cell Death Differ. *25*, 353–367.

Schweizer, U., Bohleber, S., and Fradejas-Villar, N. (2017). The modified base isopentenyladenosine and its derivatives in tRNA. RNA Biol. *14*, 1197–1208.

Seyfried, T.N., Flores, R., Poff, A.M., D'Agostino, D.P., and Mukherjee, P. (2015). Metabolic therapy: a new paradigm for managing malignant brain cancer. Cancer Lett. *356*, 289–300.

Skrtić, M., Sriskanthadevan, S., Jhas, B., Gebbia, M., Wang, X., Wang, Z., Hurren, R., Jitkova, Y., Gronda, M., Maclean, N., et al. (2011). Inhibition of mitochondrial translation as a therapeutic strategy for human acute myeloid leukemia. Cancer Cell *20*, 674–688.

Sunayama, J., Matsuda, K., Sato, A., Tachibana, K., Suzuki, K., Narita, Y., Shibui, S., Sakurada, K., Kayama, T., Tomiyama, A., and Kitanaka, C. (2010). Crosstalk between the PI3K/mTOR and MEK/ERK pathways involved in the maintenance of self-renewal and tumorigenicity of glioblastoma stem-like cells. Stem Cells *28*, 1930–1939.

Suvà, M.L., Rheinbay, E., Gillespie, S.M., Patel, A.P., Wakimoto, H., Rabkin, S.D., Riggi, N., Chi, A.S., Cahill, D.P., Nahed, B.V., et al. (2014). Reconstructing and reprogramming the tumor-propagating potential of glioblastoma stem-like cells. Cell *157*, 580–594.

Ueda, Y., Wei, F.Y., Hide, T., Michiue, H., Takayama, K., Kaitsuka, T., Nakamura, H., Makino, K., Kuratsu, J., Futaki, S., and Tomizawa, K. (2012). Induction of autophagic cell death of glioma-initiating cells by cell-penetrating D-isomer peptides consisting of Pas and the p53 C-terminus. Biomaterials *33*, 9061–9069.

Wang, H., Wei, L., Li, C., Zhou, J., and Li, Z. (2015). CDK5RAP1 deficiency induces cell cycle arrest and apoptosis in human breast cancer cell line by the ROS/JNK signaling pathway. Oncol. Rep. *33*, 1089–1096.

Wei, F.Y., Zhou, B., Suzuki, T., Miyata, K., Ujihara, Y., Horiguchi, H., Takahashi, N., Xie, P., Michiue, H., Fujimura, A., et al. (2015). Cdk5rap1-mediated 2-methylthio modification of mitochondrial tRNAs governs protein translation and contributes to myopathy in mice and humans. Cell Metab. *21*, 428–442.

Xie, P., Wei, F.Y., Hirata, S., Kaitsuka, T., Suzuki, T., Suzuki, T., and Tomizawa, K. (2013). Quantitative PCR measurement of tRNA 2-methylthio modification for assessing type 2 diabetes risk. Clin. Chem. *59*, 1604–1612.

Xie, Q., Wu, Q., Horbinski, C.M., Flavahan, W.A., Yang, K., Zhou, W., Dombrowski, S.M., Huang, Z., Fang, X., Shi, Y., et al. (2015). Mitochondrial control by Drp1 in brain tumor initiating cells. Nat. Neurosci. *18*, 501–510.

Zaidi, S.K., Grandy, R.A., Lopez-Camacho, C., Montecino, M., van Wijnen, A.J., Lian, J.B., Stein, J.L., and Stein, G.S. (2014). Bookmarking target genes in mitosis: a shared epigenetic trait of phenotypic transcription factors and oncogenes? Cancer Res. *74*, 420–425.

ISCI, Volume *21*

Supplemental Information

2-Methylthio Conversion of N6-Isopentenyladenosine in Mitochondrial tRNAs by CDK5RAP1 Promotes the Maintenance of Glioma-Initiating Cells

Takahiro Yamamoto, Atsushi Fujimura, Fan-Yan Wei, Naoki Shinojima, Jun-ichiro Kuroda, Akitake Mukasa, and Kazuhito Tomizawa

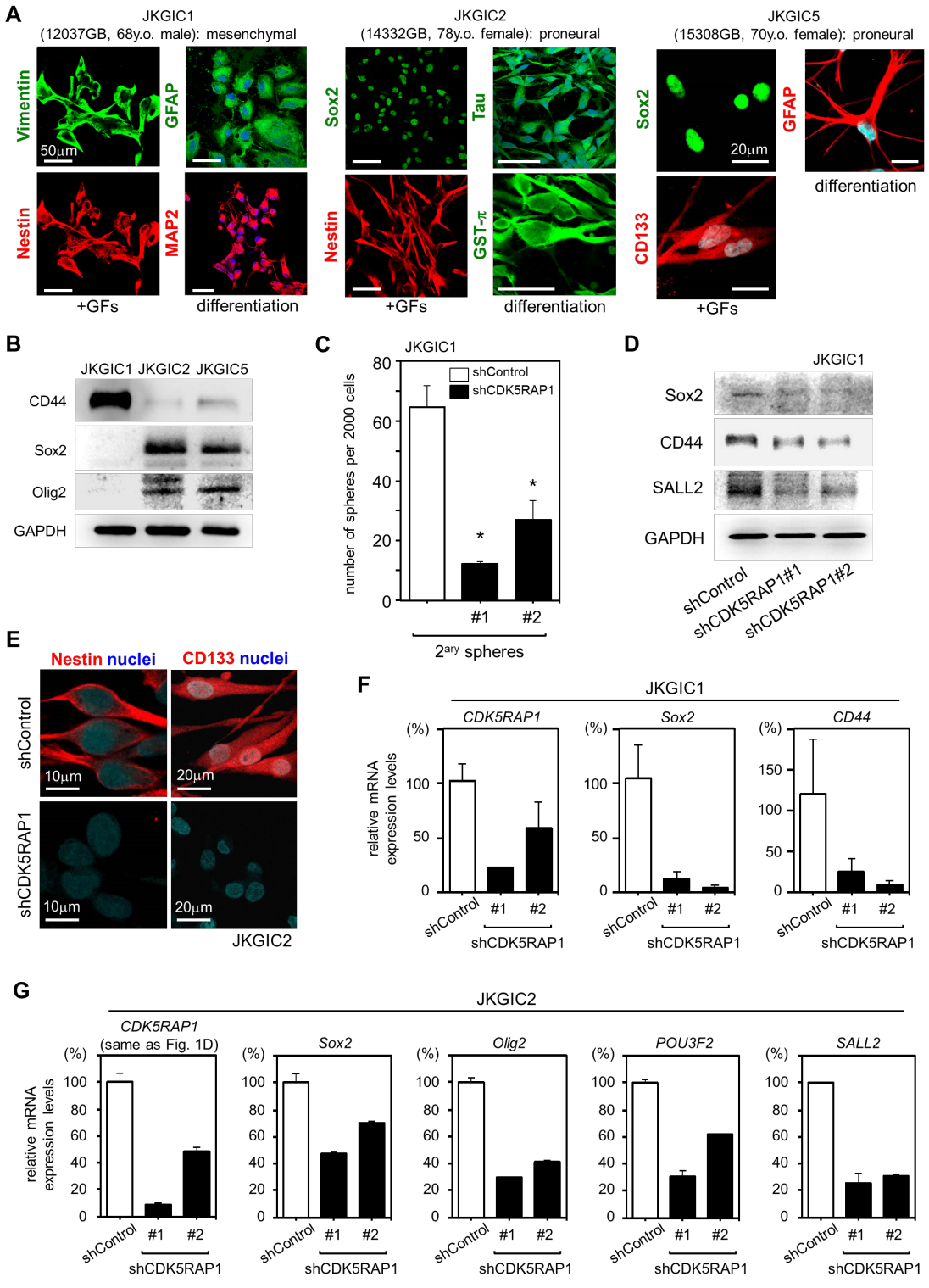
A
JKGIC1
(12037GB, 68y.o. male): mesenchymal
JKGIC2
(14332GB, 78y.o. female): proneural
JKGIC5
(15308GB, 70y.o. female): proneural
Vimentin
GFAP
Sox2
Tau
Sox2
GFAP
50μm
20μm
Nestin
MAP2
Nestin
GST-π
CD133
+GFs
differentiation
+GFs
differentiation
+GFs
differentiation
B
JKGIC1 JKGIC2 JKGIC5
CD44
Sox2
Olig2
GAPDH
C
JKGIC1
shControl
shCDK5RAP1
number of spheres per 2000 cells
80
60
40
20
0
*
*
#1
#2
2ary spheres
D
JKGIC1
Sox2
CD44
SALL2
GAPDH
shControl
shCDK5RAP1#1
shCDK5RAP1#2
E
Nestin nuclei
CD133 nuclei
shControl
shCDK5RAP1
10μm
20μm
10μm
20μm
JKGIC2
F
JKGIC1
CDK5RAP1
Sox2
CD44
(%)
relative mRNA expression levels
100
50
0
150
shControl
#1
#2
shCDK5RAP1
G
JKGIC2
CDK5RAP1
(same as Fig. 1D)
Sox2
Olig2
POU3F2
SALL2
(%)
relative mRNA expression levels
100
80
60
40
20
0
shControl
#1
#2
shCDK5RAP1

Figure S1. CDK5RAP1 is required to sustain the GIC-related traits and the transcriptional regulation of the GIC markers. (related to Figure 1).

(A-B) Molecular characteristics of JKGIC1, JKGIC2 and JKGIC5 cells. (A) Immunocytochemical analysis for GIC (Vimentin, Sox2, Nestin and CD133), neural (MAP2 and Tau), astrocytic (GFAP) and oligodendrocytic (GST-π) markers. (B) Western blotting for CD44, Sox2, and Olig2 in each cell. CD44 is abundantly expressed in JKGIC1 cells, whereas Sox2 and Olig2 are predominately expressed in JKGIC2 and JKGIC5 cells. All cell lines can differentiate into several lineages, such as neuronal, astrocytic and oligodendrocytic lineages.

(C) Quantification of secondary sphere formation by shControl-, shCDK5RAP1#1-, and shCDK5RAP1#2-transfected JKGIC1 cells. CDK5RAP1 is required to sustain the anchorage-independent growth capacity of JKGIC1 cells. The data are presented as the number of spheres formed from 2,000 seeded cells. Each bar represents the SD value from four independent replicates. *: $P<0.05$ *vs.* shControl.

(D) CDK5RAP1 knockdown decreases the expression levels of transcriptional regulators of GIC markers in JKGIC1.

(E) Representative immunostaining images for each stem cell marker in shControl- and shCDK5RAP1-transfected JKGIC2 cells. Cells were dispersed on Matrigel® Matrix (Corning, Bedford, MA), and then immunocytochemical analysis was performed. CDK5RAP1 deficiency results in reduced staining for Nestin and CD133.

(F-G) CDK5RAP1 deficit reduces the expression levels of GIC-related transcriptional factors in JKGIC1 and JKGCI2. Each bar represents the SD value from three independent replicates.

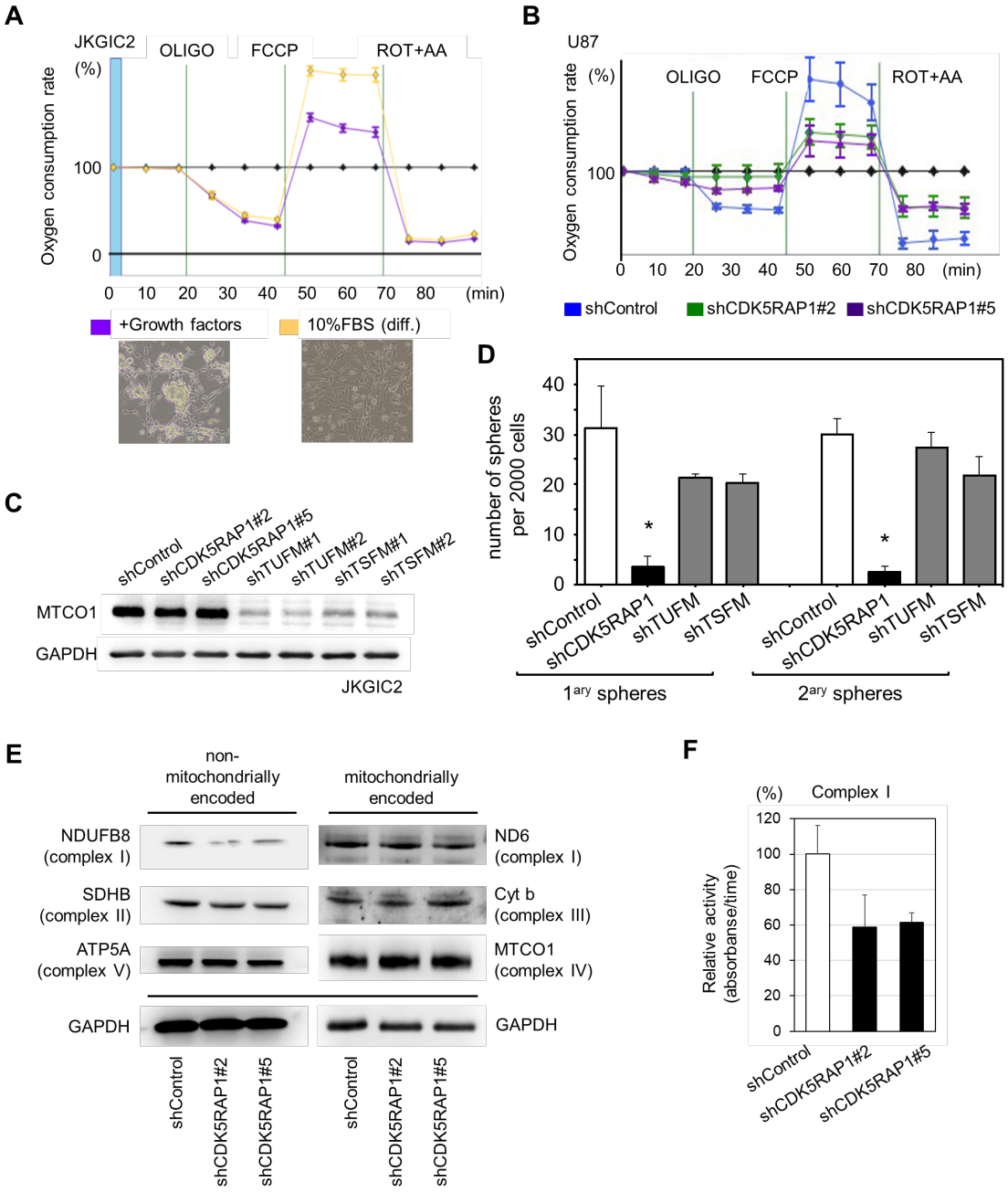
A
JKGIC2
OLIGO
FCCP
ROT+AA
(%)
Oxygen consumption rate
100
0
0 10 20 30 40 50 60 70 80 (min)
+Growth factors
10%FBS (diff.)
B
U87
(%)
OLIGO
FCCP
ROT+AA
Oxygen consumption rate
100
0 10 20 30 40 50 60 70 80 (min)
shControl
shCDK5RAP1#2
shCDK5RAP1#5
C
shControl
shCDK5RAP1#2
shCDK5RAP1#5
shTUFM#1
shTUFM#2
shTSFM#1
shTSFM#2
MTCO1
GAPDH
JKGIC2
D
number of spheres per 2000 cells
40
30
20
10
0
*
*
shControl
shCDK5RAP1
shTUFM
shTSFM
shControl
shCDK5RAP1
shTUFM
shTSFM
1ary spheres
2ary spheres
E
non-mitochondrially encoded
mitochondrially encoded
NDUFB8 (complex I)
SDHB (complex II)
ATP5A (complex V)
GAPDH
ND6 (complex I)
Cyt b (complex III)
MTCO1 (complex IV)
GAPDH
shControl
shCDK5RAP1#2
shCDK5RAP1#5
shControl
shCDK5RAP1#2
shCDK5RAP1#5
F
(%) Complex I
Relative activity (absorbanse/time)
120
100
80
60
40
20
0
shControl
shCDK5RAP1#2
shCDK5RAP1#5

Figure S2. CDK5RAP1 controls GIC-related traits in a mitochondrial translation-independent manner (related to Figure 2).

(A) *Upper panel*: Representative oxygen consumption rates in JKGIC2 cells cultured in GIC medium containing bFGF and EGF (+GF) or differentiation medium containing 10% FBS. Upon exposure to a differentiation cue, respiratory coupling was significantly induced after FCCP treatment in differentiated JKGIC2 cells. n = 5 per condition. *Lower panel*: Representative images of undifferentiated (purple) and differentiated (orange) JKGIC2 cells.

(B) Representative oxygen consumption rates in U87MG cells transfected with shControl, shCDK5RAP1#2, or shCDK5RAP1#5. In contrast to that in JKGIC2 cells, CDK5RAP1 deficiency induced a marked change in the OCR in the non-GIC line. n=5 per condition.

(C) Immunoblots for MTCO1 in JKGIC2 cells transfected with each shRNA. GAPDH served as a loading control.

(D) Knockdown of CDK5RAP1 represses the anchorage-independent growth ability of JKGIC2 cells. In contrast, knockdown of either TUFM or TSFM has no effect on the self-renewal capacity of JKGIC2 cells. Each bar represents the SD value from four independent replicates. *: $P<0.05$ *vs.* shControl.

(E) CDK5RAP1 deficit slightly attenuated the protein level of NDUFB8, but had no effect on other component proteins in JKGIC2. Note that the levels of proteins encoded by mitochondrial genome such as ND6, cytochrome b, and MTCO1 were not reduced upon loss of CDK5RAP1.

(F) Complex I activity was reduced upon CDK5RAP1 knockdown.

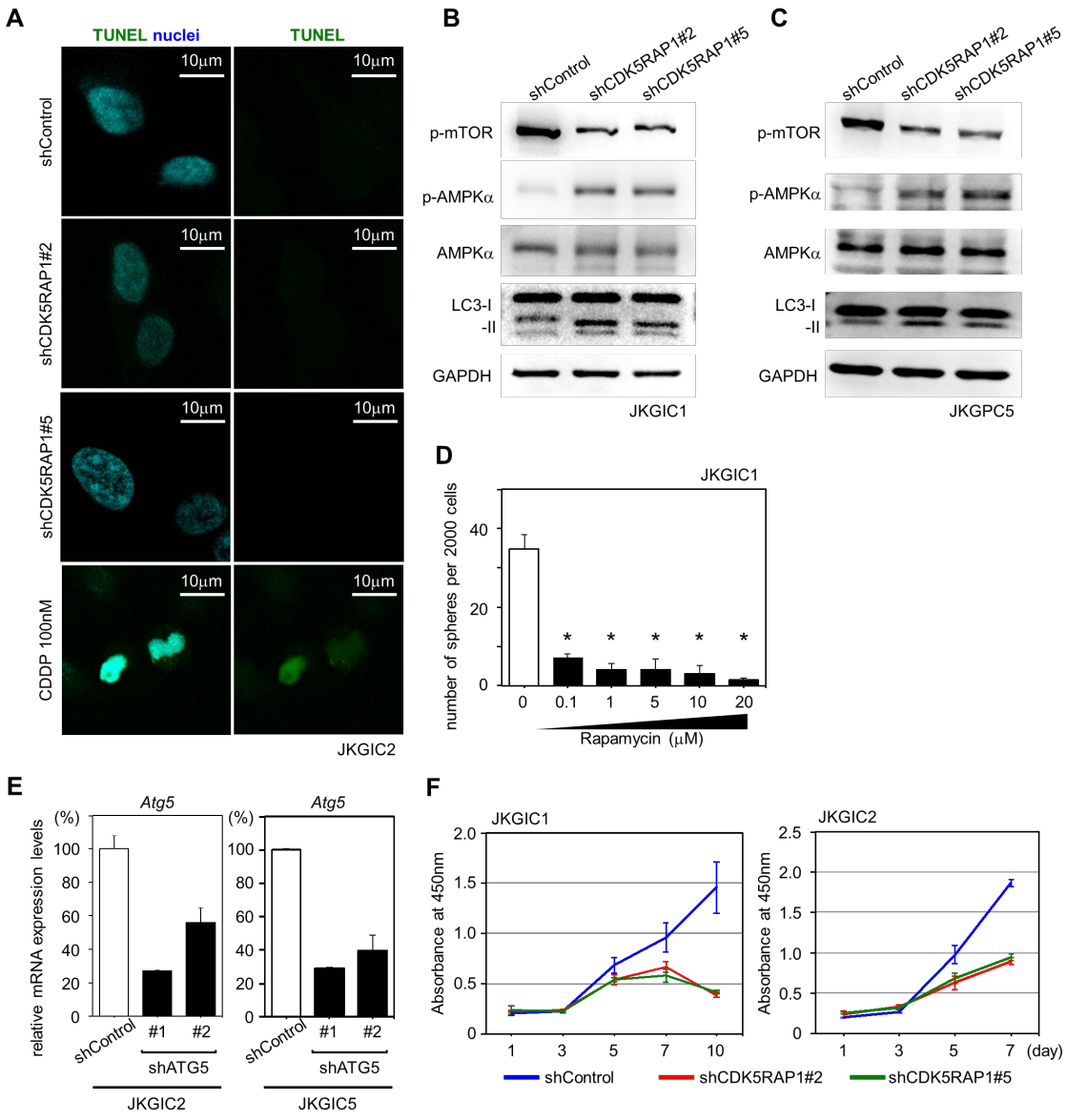

Figure S3. CDK5RAP1 knockdown inhibits the growth of GICs but does not induce apoptosis in GICs (related to Figure 3).

(A) Representative images of TUNEL assays in JKGIC2 cells transfected with shControl or shCDK5RAP1#2. Note that CDK5RAP1 knockdown does not activate apoptosis. CDDP-treated JKGIC2 cells served as a positive control for the TUNEL assay.

(B-C) Immunoblotting analyses of mTOR, AMPK, and LC3 show that CDK5RAP1 knockdown activates the autophagic program in JKGIC1 and JKGCI5 cells.

(D) Dose-dependent effect of rapamycin on the number of spheres formed from 2,000 JKGIC1 cells. Each bar represents the SD value from four independent replicates. *: $P<0.05$.

(E) The efficiency of shATG5 was examined by real-time PCR in JKGIC2 and JKGIC5 cells. n = 5 per condition.

(F) CDK5RAP1 knockdown inhibits the growth of both JKGIC1 and JKGIC2 cells. Cell growth was measured by the WST-8 assay.

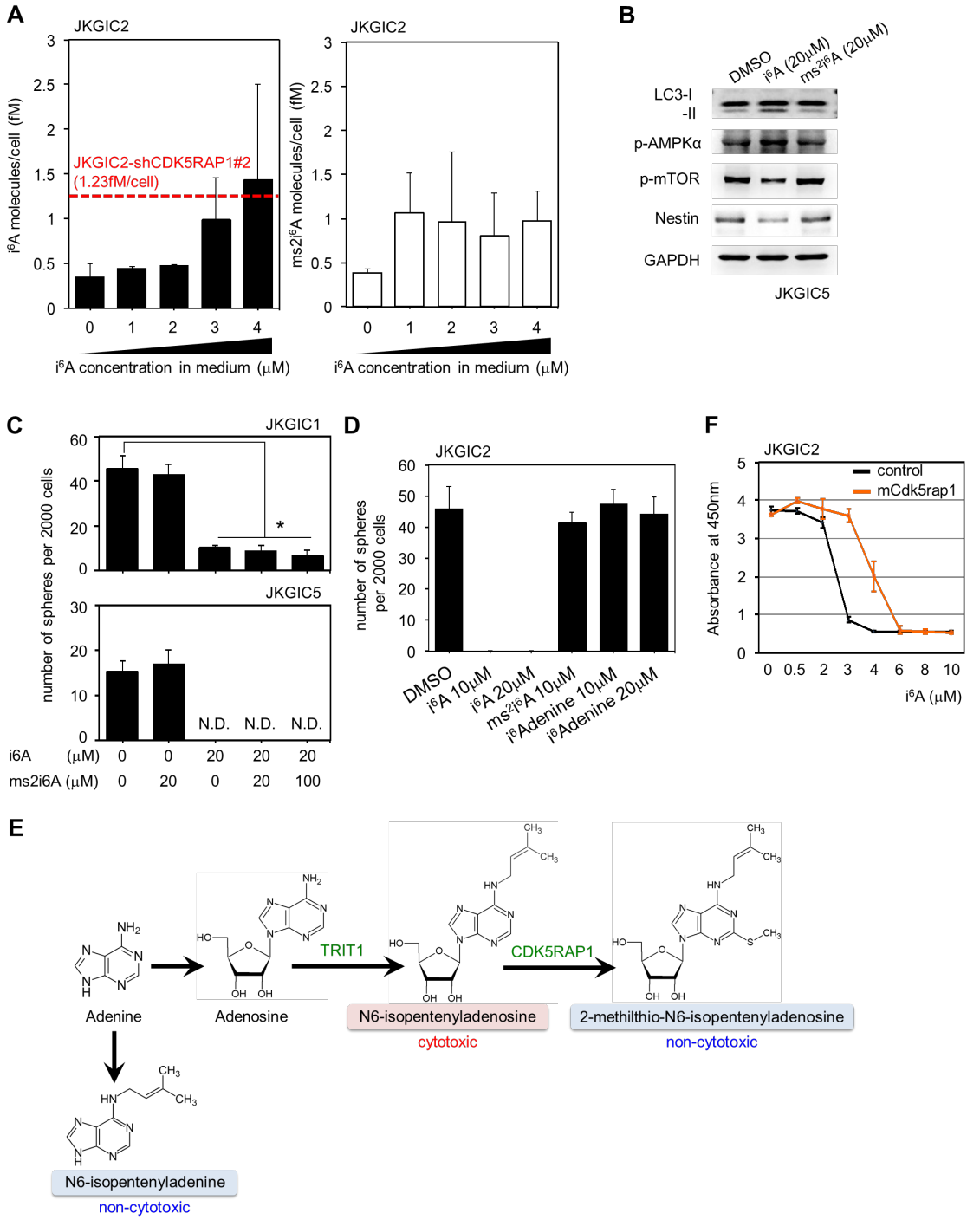
A
JKGIC2
i6A molecules/cell (fM)
JKGIC2-shCDK5RAP1#2
(1.23fM/cell)
i6A concentration in medium (μM)
JKGIC2
ms2i6A molecules/cell (fM)
i6A concentration in medium (μM)
B
DMSO
i6A (20μM)
ms2i6A (20μM)
LC3-I
-II
p-AMPKα
p-mTOR
Nestin
GAPDH
JKGIC5
C
JKGIC1
number of spheres per 2000 cells
JKGIC5
N.D.
i6A (μM)
ms2i6A (μM)
D
JKGIC2
number of spheres per 2000 cells
DMSO
i6A 10μM
i6A 20μM
ms2i6A 10μM
i6Adenine 10μM
i6Adenine 20μM
F
JKGIC2
control
mCdk5rap1
Absorbance at 450nm
i6A (μM)
E
Adenine
Adenosine
TRIT1
N6-isopentenyladenosine
cytotoxic
CDK5RAP1
2-methilthio-N6-isopentenyladenosine
non-cytotoxic
N6-isopentenyladenine
non-cytotoxic

Figure S4. Isopentenyl modification of the adenosine molecule alone results in cytotoxic effects, and i^6A is detoxified by 2-methylthio conversion via CDK5RAP1 (related to Figure 4).

(A) *Left*: i^6A treatment induced the intracellular concentration of i^6A in JKGIC2 cells in a dose-dependent manner. Note that the intracellular [i^6A] in JKGIC2 cells treated with 4 μM i^6A was consistent with that in shCDK5RAP1#2-JKGIC2 cells. *Right*: Intracellular concentration of ms^2i^6A in JKGIC2 cells treated with each concentration of i^6A. Exogenous i^6A did not affect the intracellular concentration of ms^2i^6A in a dose-dependent manner

(B) Treatment with i^6A, but not ms^2i^6A, activates the autophagic program and decreases the protein levels of Nestin in JKGIC5 cells.

(C) Quantification of primary spheres formed by JKGIC1 and JKGIC5 cells treated with i^6A or ms^2i^6A. Treatment with i^6A reduces the number of spheres, but this reduction is not rescued by the further addition of ms^2i^6A. Each bar represents the SD value from four independent replicates. *: $P<0.05$.

(D) Quantification of primary sphere formation by JKGIC2 cells (2,000/well) treated with i^6A, ms^2i^6A, and i^6Adenine. Treatment with i^6A but not ms^2i^6A or i^6Adenine reduces the number of spheres formed. Each bar represents the SD value from three independent replicates.

(E) Summary of the biochemical reactions related to the synthesis of i^6A, ms^2i^6A, and i^6Adenine.

(F) Effect of each concentration of i^6A on the growth of JKGIC2 cells overexpressing mouse Cdk5rap1 (mCdk5rap1). Overexpression of mCdk5rap1 protects cells from the inhibitory effect of 3 and 4 μM i^6A.

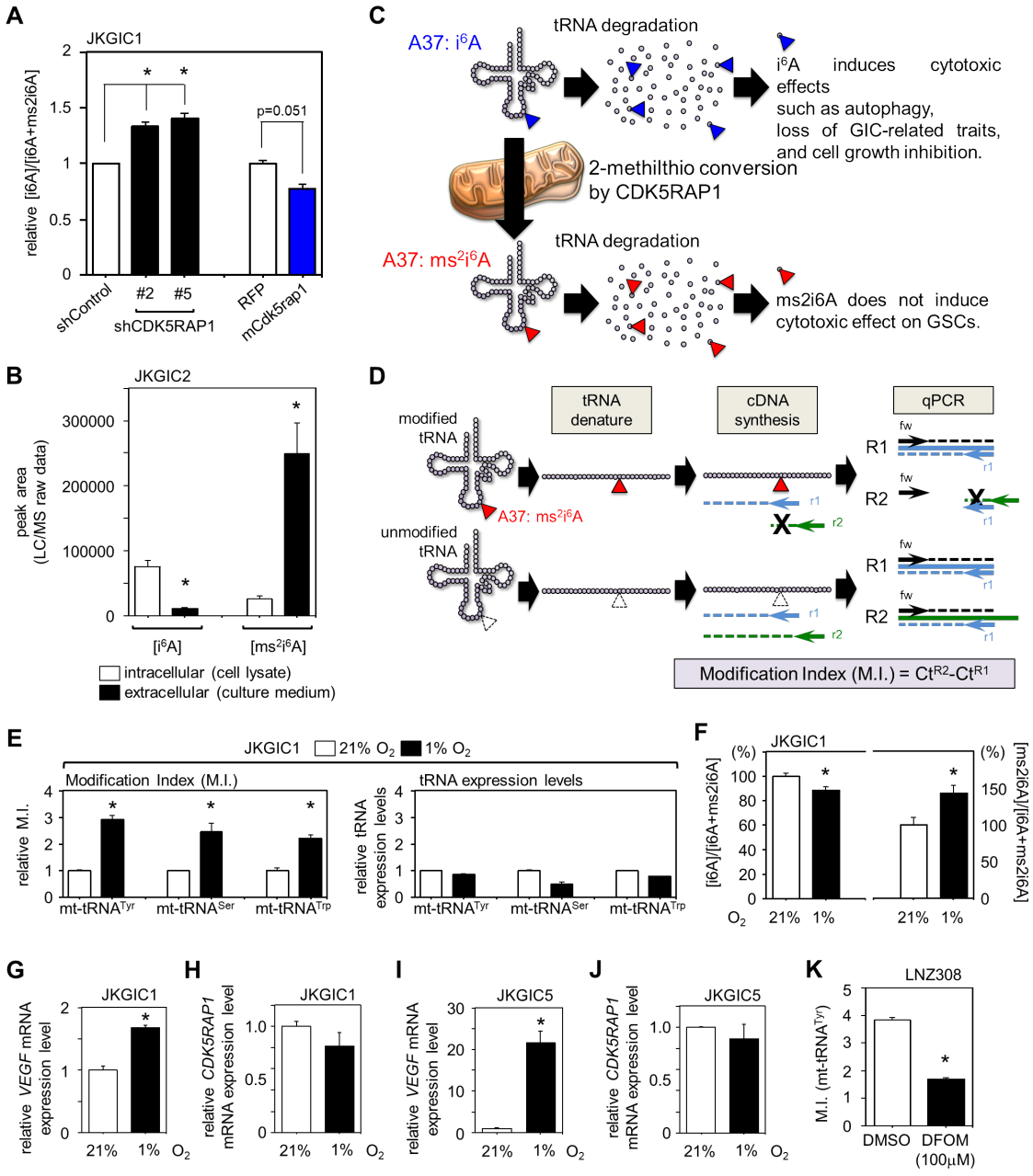
A
JKGIC1
relative [i6A]/[i6A+ms2i6A]
p=0.051
shControl
#2
#5
shCDK5RAP1
RFP
mCdk5rap1
B
JKGIC2
peak area (LC/MS raw data)
[i6A]
[ms2i6A]
intracellular (cell lysate)
extracellular (culture medium)
C
A37: i6A
tRNA degradation
i6A induces cytotoxic effects such as autophagy, loss of GIC-related traits, and cell growth inhibition.
2-methilthio conversion by CDK5RAP1
A37: ms2i6A
tRNA degradation
ms2i6A does not induce cytotoxic effect on GSCs.
D
tRNA denature
cDNA synthesis
qPCR
modified tRNA
A37: ms2i6A
unmodified tRNA
fw
R1
R2
r1
r2
Modification Index (M.I.) = CtR2-CtR1
E
JKGIC1 21% O2 1% O2
Modification Index (M.I.)
relative M.I.
tRNA expression levels
relative tRNA expression levels
mt-tRNATyr
mt-tRNASer
mt-tRNATrp
F
JKGIC1
[i6A]/[i6A+ms2i6A]
[ms2i6A]/[i6A+ms2i6A]
O2 21% 1%
G
JKGIC1
relative VEGF mRNA expression level
H
JKGIC1
relative CDK5RAP1 mRNA expression level
I
JKGIC5
relative VEGF mRNA expression level
J
JKGIC5
relative CDK5RAP1 mRNA expression level
K
LNZ308
M.I. (mt-tRNATyr)
DMSO
DFOM (100μM)

Figure S5. CDK5RAP1 controls the 2-methylthio modification of mt-tRNAs (related to Figure 5).

(A) Mass spectrometry analysis of [i^6A] and [ms^2i^6A] from the lysates of shControl- and shCDK5RAP1-, RFP-, mCdk5rap1-transfected JKGIC1 cells. Each bar represents the SD value from three independent replicates. *: $P<0.05$.

(B) LC/MS analyses of intracellular and extracellular concentrations of i^6A and ms^2i^6A. Note that ms^2i^6A is predominantly enriched in the cell culture medium. Each bar represents the SD value from three independent replicates.

(C) A model describing the molecular pathways that detoxify N6-isopentenyladenosine (i^6A). i^6A at position 37 in mt-tRNAs in the mitochondria is converted to ms^2i^6A by CDK5RAP1. Both i^6A and ms^2i^6A were produced by the degradation of mt-tRNAs.

(D) A schema describing the measurement of the M.I. of mt-tRNAs. For details, please see our previous report (Xie et al., 2013).

(E) The M.I. of ms^2i^6A corresponding each mt-tRNA, and tRNA expression level in JKGIC1 cells cultured in the presence of 21% and 1% O_2. The M.I.s in all CDK5RAP1-targeted tRNA species are increased under hypoxic conditions, but tRNA expression is not. The data are presented as the M.I. relative to the cells cultured under normoxia. Each bar represents the SD value from two independent replicates.

(F) Hypoxic conditions decrease intracellular [i^6A] and increase the secretion of ms^2i^6A by JKGIC1 cells. The data are presented as the percentage of the levels under normoxia. Each bar represents the SD value from three independent replicates. *: $P<0.05$.

(G-J) Hypoxic conditions significantly increased the expression levels of *VEGF* mRNA (G and I) but not *CDK5RAP1* mRNA (H and J) in JKGIC1 and JKGIC5 cells. Each bar represents the SD value from four independent replicates. *: $P<0.05$.

(K) Representative M.I. in LNZ308 cells treated with deferoxamine (100 μM). Each bar represents the mean of four replicates ± SD. *: $P<0.05$ *vs.* DMSO.

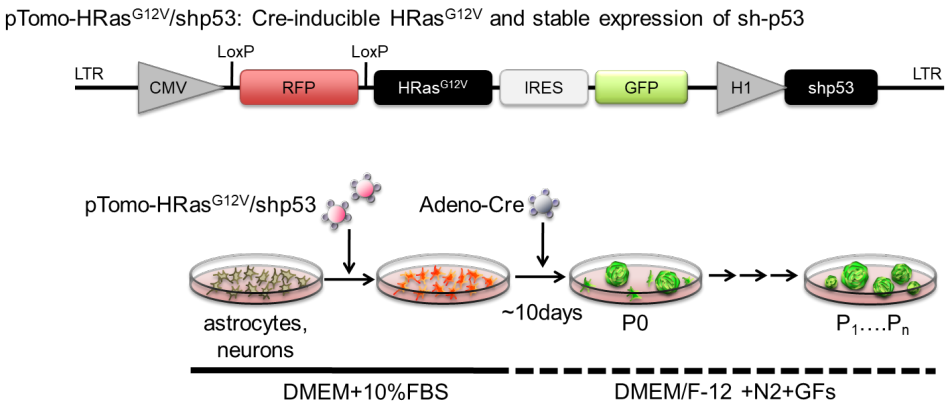

Figure S6. A schema representing the procedure of the gliosphere initiation assay (related to Figure 6).

TRANSPARENT METHODS

Cell Lines and Culture

Japan Kumamoto glioma-initiating cell (JKGIC) lines 1, 2, and 5 were used; these are patient-derived cell lines established at the Department of Neurosurgery, Kumamoto University Hospital. JKGIC1 cells were obtained from a 68-year-old male GBM patient, JKGIC2 cells were obtained from a 78-year-old female GBM patient, and JKGIC5 cells were obtained from a 70-year-old female GBM patient. The patients underwent tumor resection at our department, and primary GICs were cultured from the tumors. The tumors were washed with PBS (Thermo Fisher Scientific, Waltham, MA), cut into small pieces and minced. The minced tumors were subjected to trypsinization with 0.05% trypsin-EDTA (Wako, Tokyo, Japan) for 10 min at 37°C and plated. Study approval was obtained from the research ethics committee of Kumamoto University (Approval number: genome 231). GICs were grown in DMEM/Ham's F-12 with L-glutamine (Wako) supplemented with 10% BIT9500 (STEMCELL Technologies, Vancouver, Canada), 20 ng/ml basic fibroblast growth factor (Wako), 20 ng/ml epidermal growth factor (Wako), and 100 U/ml penicillin and streptomycin (Thermo Fisher Scientific) at 37°C in an environment containing 5% CO_2.

Xenograft experiments with patient-derived GICs.

For the xenograft tumor models, we used patient-derived GICs. We injected cells into 6-week-old female ICR-nu nu/nu mice and 6-week-old male BALB/c-nu

(CAnN.Cg-Foxn1^{nu}/CrlCrl)) mice to establish intracranial tumor xenograft models and subcutaneous xenograft models, respectively (all mice were obtained from Charles River Laboratories Japan, Yokohama, Japan). For the Kaplan-Meier analysis of survival, we defined endpoints as the time when the mice began to display neurological dysfunctions such as hemiparesis, were moribund or exhibited more than 20% weight loss. All procedures were approved by the Animal Ethics Committee of Kumamoto University (Approval ID: A29-016).

To generate the subcutaneous tumor xenograft model, we transduced JKGIC1, JKGIC2, and JKGIC5 cells with lentiviral vectors expressing shCDK5RAP1 or shControl. Equal numbers of cells (5 X 10^6 cells/100 μl) in PBS with 50% Matrigel® Matrix (Corning, Bedford, MA) were injected into both flanks (100 μl/side).

To generate the intracranial tumor xenograft model, we transduced JKGIC2 cells with lentiviral vectors expressing shCDK5RAP1 or shControl. The cells were diluted to equal concentrations (1 X 10^5 cells/μl) in PBS. At 1 to 2 weeks before cell injection, an implantable guide-screw system for intracranial injection was established as previously described (Lal et al., 2000). A 2.6-mm guide screw was implanted into a cranial hole made 2.5 mm lateral and 1 mm anterior to the bregma. Cells were injected (5 μl/hole of the guide screw) using a Hamilton syringe (Hamilton, Reno, Nevada).

Human Tissue Sample Collection and Studies

Tumor and peritumor (adjacent normal) tissues were collected from GBM patients treated at Kumamoto University Hospital. Tissues were used to assess gene expression levels, immunofluorescence staining, and mt-tRNA modifications as well as to perform LC-MS/MS. Approval was sought and obtained from the research ethics committee of Kumamoto University (Approval number: genome 231).

Mass spectrometry analysis of A, i^6A and ms^2i^6A.

Mass spectrometry analysis was performed to measure the levels of adenosine (A), N^6-isopentenyladenosine (i^6A) and 2-methylthio-N^6-isopentenyladenosine (ms^2i^6A) in the cell culture medium and tumor tissues. To extract nucleosides from the culture medium, we used a MonoSpin™ C18 (GL Sciences, Tokyo, Japan) according to the manufacturer's instructions. To extract intracellular nucleosides, we washed the cells three times with PBS and then homogenized them with 500 µl methanol. To extract nucleosides from tumor tissues, we homogenized the tissues by TissueRuptor (Qiagen, Venlo, Netherlands) in 500 µl methanol. The extracts were cleared by centrifugation at 10,000 rpm for 5 min. The supernatant was evaporated with a Savant Speed Vac SPD1010 (Thermo Fisher Scientific), and the pellet was resuspended in ultrapure water (Wako). The samples were analyzed with a triple-quadruple mass spectrometer (LCMS-8050, Shimazu, Kyoto, Japan) equipped with an electrospray ionization (ESI) source and a liquid chromatography system (Shimazu). A, i^6A and ms^2i^6A were detected by a multiple reaction monitoring (MRM) method in the positive ion mode.

The MRM parameters were as follows: A (precursor ion: m/z 268.0, product ion: m/z 136.0, collision energy: 17.0), i^6A (precursor ion: m/z 336.2, product ion: m/z 204.0, collision energy: 15.0), and ms^2i^6A (precursor ion: m/z 382.2, product ion: m/z 182.0, collision energy: 29.0).

i^6A and ms^2i^6A Treatment

GICs were seeded at approximately 80% confluence. The medium was removed and replaced with new medium containing different concentrations of i^6A (Wako) or ms^2i^6A (Wako). After 24 hours, immunocytochemical analysis was performed. Total proteins and nucleosides were extracted from cells 24 hours after i^6A and ms^2i^6A treatment. Sphere formation assays were performed one week after the treatment.

Lentiviral Preparation and Infection

Lentiviral vectors were used for gene silencing or gene expression. For lentivirus production, we cultured 293FT cells in DMEM (Thermo Fisher Scientific) supplemented with 10% FBS (Corning) and 100 U/ml penicillin and streptomycin (Thermo Fisher Scientific) at 37°C and 5% CO_2. Lentiviral vectors (10 μg) with the packaging vectors psPAX2 (7.5 μg) and pMD2.G (2.5 μg) were transiently transfected into 293FT cells using TransIT®-LT1 Transfection Reagent (Mirus Bio, Madison, WI) and Opti-MEM™ (Thermo Fisher Scientific). At 8-12 hours after transfection, the medium was changed. On the third day after transfection, viral supernatant was

collected and filtered through a 0.45 μm sterile filter unit containing a Durapore® PVDF membrane (Millipore, Darmstadt, Germany). Approximately 500-1,000 μl viral supernatant was used to infect GICs in a 25 cm^2 flask. The shRNA sequences are shown in the SUPPLEMENTAL TABLE (Table S1: Sequences).

Sphere Formation Assay

GICs were plated at 2,000 cells per well and grown at 37°C in an atmosphere containing 5% CO_2. After 1 week, the number of spheres per well (from 2,000 cells) was counted. To distinguish between independent spheres and improve our ability to count the number of spheres, we used ultra-low attachment 24-well plates (Corning). After the primary assay, the cells were replated at 2,000 cells per well, and secondary sphere formation assays were performed. For each condition, we prepared 4 technical replicates and performed 3 independent experiments unless otherwise noted.

Immunofluorescence Staining

Tissues were fixed overnight in formalin, embedded in paraffin and sliced into 4-μm-thick sections. After deparaffinization, Protease XXV (Thermo Fisher Scientific) was added to the sections for antigen retrieval, and the sections were then processed for immunofluorescence staining. The cells were fixed for 15 min at room temperature with 4% PFA, after which they were subjected to the following process: blocking with 5% donkey serum in PBST (0.2% Triton X-100 in PBS) for 1 hour at room temperature,

incubation with primary antibodies diluted with 5% donkey serum in PBST at 4°C overnight, and incubation with secondary antibodies diluted with 5% donkey serum in PBST at room temperature for 2 hours. The dilutions of primary and secondary antibodies were set according to the manufacturers' instructions. To label cell nuclei, we counterstained the samples with ProLong™ Gold Antifade Mountant with DAPI (Thermo Fisher Scientific). Images were obtained with an FV3000 confocal microscope (Olympus, Tokyo, Japan). A Fluorescein *In Situ* Cell Death Detection Kit (Sigma-Aldrich, St. Louis, Missouri) was used for the detection of apoptosis based on labeling of DNA strand breaks (TUNEL). The antibodies used are shown in the SUPPLEMENTAL TABLE (Table S2: Antibodies). For each experiment, we prepared 2 technical replicates and performed at least 2 independent experiments unless otherwise noted.

Immunoblotting (Western Blotting)

Proteins were extracted from cells with lysis buffer (20 mM Tris-HCL (pH 7.5), 1 mM EDTA-2Na, 1% Triton X-100, and PhosSTOP cocktail (1 tablet/10 ml)). The collected and lysed cells were homogenized with SONIFIER 250 (BRANSON, Danbury, CT) and cleared by centrifugation at 15,000 rpm and 4°C for 15 min. Protein concentrations were determined using a Pierce™ BCA Protein Assay Kit (Thermo Fisher Scientific). Equal amounts of proteins were electrophoresed on a 6-12% gradient acrylamide gel with Precision Plus Protein™ Dual Color Standards (Bio-Rad, Hercules, CA) and

transferred to PVDF membranes (Millipore). The membranes were blocked with 0.5% skim milk in TBST at room temperature for 1 hour, and blotting was performed by incubating the membranes with primary antibodies at 4°C overnight. Secondary antibodies were then incubated with the membranes at room temperature for 1 hour. Detection was performed with Amersham™ ECL™ Prime Western Blotting Detection Reagent (GE Healthcare, Fairfield, CT). The dilutions of the primary and secondary antibodies were used according to the manufacturers' instructions. The antibodies used are shown in the SUPPLEMENTAL TABLE (Table S2: Antibodies). We performed at least 2 independent experiments unless otherwise noted.

RNA Isolation and Quantitative RT-PCR

Total RNA from cells and tissues were isolated using TRIzol reagent (Thermo Fisher Scientific) and processed according to the manufacturer's instructions. The isolated RNA was diluted to 50 ng/μl. Recombinant DNase I (Takara, Shiga, Japan) was added to the isolated RNA and incubated for 20 min at 37°C. The RNA was then reverse-transcribed into cDNA using PrimeScript™ RT Master Mix (Takara). Quantitative RT-PCR was performed using gene-specific primers and SYBR Premix Ex Taq™ (Takara). The sequences of gene-specific primers (18S as a reference) are shown in the SUPPLEMENTAL TABLE (Table S1: Sequences). For each condition, we prepared 2 technical replicates and performed 2 independent experiments unless otherwise noted.

Modification Index of mitochondrial tRNA

To determine the ms^2i^6A modification in mitochondrial tRNAs, we adopted the quantitative PCR-based method, which we previously reported (Xie et al., 2013). Briefly, DNase I-treated total RNA were denatured at 65°C for 10min, and were used for cDNA synthesis with mitochondrial tRNA-specific primers (reverse r1 or reverse r2). Then, qPCR was performed with a primer set of forward (fw) and reverse r1 (rev1). The Ct number was obtained from the qPCR with cDNA templates of fw/rev1 and fw/rev2. The difference of the number of Ct(fw/rev1) and Ct(fw/rev2) is defined as the M.I. We reported that the M.I. reflected the absolute quantification of ms2 measured by mass-spectrometry.

Histology

Tumor and brain tissues were fixed overnight in formalin, embedded in paraffin and sliced into 4-μm-thick sections for histological examination. Hematoxylin and eosin (H&E) staining was performed with a standard method.

Assays to examine mitochondrial functions

The oxygen consumption rate (OCR) was determined with a Seahorse XF24 Analyzer (Agilent Technologies, Santa Clara, CA). JKGIC2 cells were plated at a density of 70,000 cells per well for measurement. Oligomycin (6.3 μM), FCCP (9 μM), rotenone

(5 μM) and antimycin (5 μM) were used as metabolic inhibitors. All assays were performed according to the manufacturer's instructions.

Electron microscopy

JKGIC2 cells were transduced with lentiviral vectors expressing shCDK5RAP1 or shControl. At 4 days after infection, the cells were fixed with 2% glutaraldehyde and 2% paraformaldehyde, further fixed with osmium tetroxide, embedded in epoxy resin, sliced, and examined with an electron microscope (HITACHI Electron Microscope Model H-7650).

Quantification and statistical analyses.

The data were analyzed using Microsoft Excel (Microsoft, Washington), GraphPad Prism (GraphPad, La Jolla, CA) and StatMate III (ATMS, Tokyo, Japan) software. Data are expressed as the mean ± SD. Student's *t* test was used to assess the differences between two groups. One-way analysis of variance (ANOVA) was used to assess the differences among multiple groups followed by t-test with Bonferroni correction of the *P* value between two groups. The log-rank test and Kaplan-Meier method were used to compare the survival distributions between two groups. $P < 0.05$ was considered statistically significant.

SUPPLEMENTAL REFERENCES

Xie, P., Wei, F.Y., Hirata, S., Kaitsuka, T., Suzuki, T., Suzuki, T., Tomizawa, K. (2013). Quantitative PCR measurement of tRNA 2-methylthio modification for assessing type 2 diabetes risk. Clin Chem 59, 1604-1612.

Murata, H., Yoshimoto, K., Hatae, R., Akagi, Y., Mizoguchi, M., Hata, N., Kuga, D., Nakamizo, A., Amano, T., Sayama, T., Iihara, K. (2015). Detection of proneural/mesenchymal marker expression in glioblastoma: temporospatial dynamics and association with chromatin-modifying gene expression. J. Neurooncol 125:33-41.

Table S1. Sequences of Primer and shRNA. Related to methods.

The ribosomal 18S gene was used as a reference gene for quantitative RT-PCR.

Primers	Sequences
Cdk5rap1 (Human) forward	ATGGCTGCCAGATGAATGTGA
Cdk5rap1 (Human) reverse	CTCTTGGAGGTTACTGGTCCG
Cdk5rap1 (Mouse) forward	CCATGTGCTGGGTGTTGCTTA
Cdk5rap1 (Mouse) reverse	TCTGCCTTCCTAGAAGTTCATCC
18S forward	GTAACCCGTTGAACCCCATT
18S reverse	CCATCCAATCGGTAGTAGCG
Sox2 forward	TACAGCATGTCCTACTCGCAG
Sox2 reverse	GAGGAAGAGGTAACCACAGGG
Olig2 forward	TGGCTTCAAGTCATCCTCGTC
Olig2 reverse	ATGGCGATGTTGAGGTCGTG
POU3F2 forward	CGGCGGATCAAACTGGGATTT
POU3F2 reverse	TTGCGCTGCGATCTTGTCTAT
SALL2 forward	CCCCTGATCTTGGAAGAGCTA
SALL2 reverse	CACCGTCTGGCCTAAGGAG
CD44 forward	TCCAACACCTCCCAGTATGACA
CD44 reverse	GGCAGGTCTGTGACTGATGTACA
CD133 forward	TTCTTGACCGACTGAGACCCA
CD133 reverse	TCATGTTCTCCAACGCCTCTT
VEGF forward	AGGGCAGAATCATCACGAAGT
VEGF reverse	AGGGTCTCGATTGGATGGCA
DLL3 forward	ACATGTGCAGATGGACCCTG
DLL3 reverse	AAAAGGTAGCGCTGAGGGTC
BCAN forward	ACCTAGCATCCCCATCACCT
BCAN reverse	GAAGTCCTGTTCCTCGGGTG
NCAM1 forward	CCTATCCCAGTGCCACGATC
NCAM1 reverse	ATCCTCTCCCATCTGCCCTT
NKX2.2 forward	ACCAACACAAAGACGGGGTT
NKX2.2 reverse	TGTAGCGGTGGTTCTGGAAC
ASCL1 forward	CAGCCTGTTTCTTTGCCACG

ASCL1 reverse	GTCGTTGGAGTAGTTGGGGG
CHI3L1 forward	TACGGCATGCTCAACACACT
CHI3L1 reverse	TGCCCATCACCAGCTTACTG
VIM forward	CTCTGGCACGTCTTGACCTT
VIM reverse	ACGAAGGTGACGAGCCATTT
RelB forward	CATCAGAGCTGCGGATTTGC
RelB reverse	GACACGGTGCCAGAGAAGAA
TRADD forward	CAGCAGAAGGTGGCAGTGTA
TRADD reverse	CACCTTGCGCCATTTGAGAC
PDPN forward	AGGTGCCGAAGATGATGTGG
PDPN reverse	GCGAGTACCTTCCCGACATT
mt-tRNATyr forward	GCTGAGTGAAGCATTGGACT
mt-tRNATyr reverse r1	AACCCCTGTCTTTAGATTTACA
mt-tRNATyr reverse r2	AGAGGCCTAACCCCTGTCTT
mt-tRNASer forward	GAGGCCATGGGGTTGG
mt-tRNASer reverse r1	CCCAAAGCTGGTTTCAAGC
mt-tRNASer reverse r2	AATCGAACCCCCCAAAGC
mt-tRNATrp forward	GGTTAAATACAGACCAAGAGC
mt-tRNATrp reverse r1	CAACTTACTGAGGGCTTTGAA
mt-tRNATrp reverse r2	TTAAGTATTGCAACTTACTGAGG
shRNA	**Sequences**
shCDK5RAP1 #1 (Human)	CCGGGGCTTTACCACCAACTATAAACTCGAGTTTATAGTTGG TGGTAAAGCCTTTTT
shCDK5RAP1 #2 (Human)	CCGGCCAATCTCAGTCGTGGCTTTACTCGAGTAAAGCCACGA CTGAGATTGGTTTTT
shCDK5RAP1 #5 (Human)	CCGGTGGAGTTAGTTCACCATATTACTCGAGTAATATGGTGA ACTAACTCCATTTTT

shTUFM #1 (Human)	CCGGGCTCACCGAGTTTGGCTATAACTCGAGTTATAGCCAAACTCGGTGAGCTTTTT
shTUFM #2 (Human)	CCGGCAGCCAATGATCTTAGAGAAACTCGAGTTTCTCTAAGATCATTGGCTGTTTTT
shTSFM #1 (Human)	CCGGCTCCTTTGTAAATTGCAAGAACTCGAGTTCTTGCAATTTACAAAGGAGTTTTT
shTSFM #2 (Human)	CCGGCAGGAAGGAAACACAACTGTACTCGAGTACAGTTGTGTTTCCTTCCTGTTTTT
shAtg5 #1 (Human)	CCGGCCTGAACAGAATCATCCTTAACTCGAGTTAAGGATGATTCTGTTCAGGTTTTT
shAtg5 #2 (Human)	CCGGCCTTTCATTCAGAAGCTGTTTCTCGAGAAACAGCTTCTGAATGAAAGGTTTTT

Table S2. The antibodies used. Related to methods.

Antibodies	SOURCE	IDENTIFIER	Dilutions
Anti-GAPDH	Santa Cruz Biotechnology	Catalog # sc-47724	WB (1:1000)
Anti-Nestin	Sigma-Aldrich	Catalog # N5413	WB (1:1000) IF (1:200)
Anti-Sox2	Santa Cruz Biotechnology	Catalog # sc-17320	WB (1:1000) IF (1:100)
Anti-Olig2	R&D Systems	Catalog # AF2418	WB (1:1000)
Anti-Brn2/POU3F2	Cell Signaling Technology	Catalog # 12137S	WB (1:1000)
Anti-SALL2	Bethyl	Catalog # A303-208A	WB (1:1000)
Anti-YAP/TAZ	Cell Signaling Technology	Catalog # 8418	IF (1:100)
Anti-MTCO1	Abcam	Catalog # ab14705	WB (1:1000)
Anti-Cleaved Caspase-3	Cell Signaling Technology	Catalog # 9661	WB (1:1000)
Anti-mTOR	Cell Signaling Technology	Catalog # 2983	WB (1:1000)
Anti-mTOR, phospho	Cell Signaling Technology	Catalog # 2976	WB (1:1000)
Anti-p70 S6 Kinase	Cell Signaling Technology	Catalog # 2708	WB (1:1000)
Anti-p70 S6 Kinase, phospho	Cell Signaling Technology	Catalog # 9208S	WB (1:1000)
Anti-Human LC3	MBL International	Catalog # PM036	WB (1:1000) IF (1:200)
Anti-AMPK alpha	Cell Signaling Technology	Catalog # 2535	WB (1:1000)
Anti-AMPK-alpha, phospho	Cell Signaling Technology	Catalog # 5831	WB (1:1000)
Anti-ms^2i^6A	Millipore	Catalog # MABS1280	IF (1:100)
Anti-Cytochrome b	Santa Cruz	Catalog # sc-9509	WB (1:1000)

Anti-ND6	Santa Cruz	Catalog # sc20510-R	WB (1:1000)
Anti-Mouse IgG	Dako	Catalog # P0447	WB (1:2000)
Anti-Rabbit IgG	Thermo Fisher Scientific	Catalog # P2771MP	WB (1:2000)
Anti-Goat IgG	Dako	Catalog # P0449	WB (1:2000)
Anti-Goat IgG, Alexa Fluor 555	Thermo Fisher Scientific	Catalog # A-21432	IF (1:500)
Anti-Rabbit IgG, Alexa Fluor 488	Thermo Fisher Scientific	Catalog # A-11034	IF (1:500)
Anti-Rabbit IgG, Alexa Fluor 555	Thermo Fisher Scientific	Catalog # A-21429	IF (1:500)
Anti-Mouse IgG, Alexa Fluor 488	Thermo Fisher Scientific	Catalog # A-11029	IF (1:500)